Front. Phys. China, 2009, 4(1): 21–37
DOI 10.1007/s11467-009-0010-1

REVIEW ARTICLE

Hua WEI (魏华), Zhi-jiao DENG (邓志娇), Wan-li YANG (杨万里), Fei ZHOU (周飞)

Cavity quantum networks for quantum information processing in decoherence-free subspace

Abstract We give a brief review on the quantum information processing in decoherence-free subspace (DFS). We show how to realize the initialization of the entangled quantum states, information transfer and teleportation of quantum states, two-qubit Grover search and how to construct the quantum network in DFS, within the cavity QED regime based on a cavity-assisted interaction by single-photon pulses.

Keywords cavity quantum network, decoherence-free subspace, quantum information processing

PACS numbers 03.67.Hk, 42.50.Dv

Contents

Hua WEI (魏华)[1, 2](✉), Zhi-jiao DENG (邓志娇)[1, 3], Wan-li YANG (杨万里)[1], Fei ZHOU (周飞)[1]

[1] State Key Laboratory of Magnetic Resonance and Atomic and Molecular Physics, Wuhan Institute of Physics and Mathematics, Chinese Academy of Sciences, Wuhan 430071, China
[2] Centre for Modern Physics and Department of Physics, Chongqing University, Chongqing 400044, China
[3] Department of Physics, National University of Defense Technology, Changsha 410073, China
E-mail: huawei.hw@gmail.com

Received November 21, 2008; accepted December 20, 2008

1 Introduction

From the latter half of the twentieth century, computer science and information theory's gradual combination into quantum mechanics began to lead to the birth of quantum computation and quantum information, especially after Gordon Moore stated his Moore's law in 1965. Quantum mechanics has been playing a more and more important role following the development of smaller and smaller electronic devices. Motivated by Deutsch's introduction of the quantum mechanics principles into the circuit and logic gates [1], the research of quantum computation and quantum information reached a full-on outbreak when Shor [2] demonstrated in 1994 that factoring large numbers could be solved efficiently on a quantum computer. Furthermore, in the succeeding year, Grover [3] demonstrated a search could be sped up by a quantum computer in a disordered database.

The stirring power of a quantum computer far more than its classical counterparts focused much attention on the physical realizations on which the quantum computation can run, and a criterion for the physical implementation of quantum computation was summarized by DiVincenzo in 2000 [4]. The research and development of quantum information processing (QIP) guided the focus of the corresponding study on the single quantum system. Many techniques for controlling single quantum systems have been developed since the 1970s. These include ion trap [5−7], photonic qubits with linear optical devices [8], nuclear magnetic resonance [9, 10], super-

conducting Josephson-junction devices [11] and quantum dot system [12]. One of the surprisingly attractive methods is trapping and manipulating a single atom/ion in an atom/ion trap inside the cavity quantum electrodynamics regime (QED) [13]. The confined single atoms isolated from the rest of the environment in the cavity QED system can keep the information encoded in its levels for a very long time. one of the most important application of the cavity-embedded single atoms is to establish a scalable distributed quantum cavity network [14]. The fixed single atoms act as the static qubits, and the communication among them is finished by the flying single-photons. Thus the difficulty of discrimination for each qubit locally is avoided and the interactions between qubits are accomplished in a nonlocal form.

However, the qubits, which are so fragile, can be easily damaged by the noise from the inevitable interaction with the environment. That's why physicists were looking for further protection techniques for the qubits. To resist decoherence, generally speaking, the qubits can be error correction coded [15], error protection coded [16], and dynamically decoupled from the environment [17]. The technology of qubit encoded in decoherence-free subspace (DFS) [16, 19, 20] belongs to the error protection encoding scheme. In DFS, the logic qubits encoded by two physical qubits

$$\begin{aligned} |\widetilde{0}\rangle &\equiv |1\rangle_1|0\rangle_2 = |10\rangle \\ |\widetilde{1}\rangle &\equiv |0\rangle_1|1\rangle_2 = |01\rangle \end{aligned} \tag{1}$$

with $|1\rangle$ and $|0\rangle$ the up and down states, respectively, of the two-level system, can resist efficiently the unpredictable imperfection, such as ambient magnetic fluctuation. The fluctuation of the environment make the phase difference, which uniquely belongs to the quantum system, between the level encoded qubits

$$\mathrm{e}^{-\mathrm{i}(E_0-E_1)t/\hbar}|0\rangle + |1\rangle \tag{2}$$

then the additional phase error can destroy the the QIP, but the logic qubits in DFS are immune to this kind of error, i.e.,

$$\begin{aligned} &\mathrm{e}^{-\mathrm{i}(E_0-E_1)t/\hbar}|1\rangle_1|0\rangle_2 + \mathrm{e}^{-\mathrm{i}(E_0-E_1)t/\hbar}|0\rangle_1|1\rangle_2 \\ &= \mathrm{e}^{-\mathrm{i}(E_0-E_1)t/\hbar}(|\widetilde{0}\rangle + |\widetilde{1}\rangle) \end{aligned} \tag{3}$$

the fluctuation of the environment cannot produce the phase error between the logic qubits. QIP in DFS is a promising scheme and it has potential applications.

In this paper, we mostly focus on the operations of the logic qubits including the preparation of entangled states, information transfer and teleportation of quantum states, two-qubit Grover search and how to construct the quantum network in DFS, within the cavity QED regime based on a cavity-assisted interaction by single-photon pulses.

2 Quantum state initialization in DFS

According to the DiVincenzo's criterion [4], the quantum state of the physical system should be easily initialized. Various quantum entangled states play a crucial role in the quantum computing and quantum information science. Besides the Bell state of two particles, the descriptions for the entangled state of multiparticles are varied. Take Greenberger-Horne-Zeilinger (GHZ) state [21], W state [22] and cluster state [23, 24] for example. They have different functions in QIP, respectively. GHZ state is the maximal entangled state of multiparticle [21], while it is more fragile than W state which can still be kept in the maximal entanglement when any one qubit is lost [22]. Cluster state is a special kind of entangled resource processed in one-way condition and only needs a sequence of one-qubit projective measurements [23, 24].

We give the example on how to generate W state, GHZ state and cluster state initialization of four remote logic-qubits in DFS [28].

First, we review the main idea of using cavity-assisted photon scattering to realize a controlled phase gate between two atoms. The key point can be viewed briefly as follows. Two identical three-level atoms are well located in a high-finesse single-mode cavity. The cavity mode, input photon pulse and the transition between the levels $|0\rangle$ and $|e\rangle$ of the atom are resonantly coupled, while level $|1\rangle$ is decoupled because of the large detuning. Because the cavity mode is h polarized, it only interacts with the h component of an input photon, as shown in Fig. 1. Under the special condition, that is, the duration of the input photon pulse T is sufficiently long and the atom-cavity coupling is much stronger than both the cavity decay and spontaneous emission of the atomic state, the pulse in resonance with the bare cavity mode, responsible for the two atoms in the state $|1\rangle_1|1\rangle_2$, would yield the pulse shape almost unchanged but with a π phase

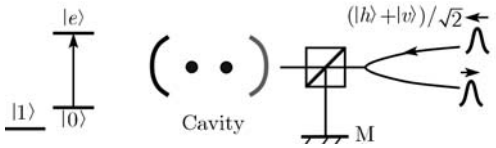

Fig. 1 **Left**: Level configuration of an atom in our scheme, where the two ground states $|0\rangle$ and $|1\rangle$ with physical qubits encoded are of large energy splitting, and $|e\rangle$ is the excited state. **Right**: Two identical atoms are well located in a high-finesse single-mode cavity to implement a two-atom U_{CPF} by cavity-assisted polarized-photon scattering. The polarizing beam splitter (PBS) transmits (reflects) the h (v) component of an input single-photon pulse.

added when reflected by the cavity. On the other hand, if any of the two atoms is in the state $|0\rangle$, the resonance between the cavity mode and the atom will shift the cavity mode so that the photon pulse cannot feel the cavity mode and leaves the cavity with both its shape and phase unchanged [25−27] by the cavity's reflection. Consequently, the whole physical procedure by reflecting a single-photon pulse with h polarization realizes the two-atom controlled phase gate $U_{\rm CPF} = \exp(\mathrm{i}\pi|1\rangle_{11}\langle 1| \otimes |1\rangle_{22}\langle 1|)$.

The initialization of the GHZ state is plotted in Fig. 2, where the initial state of the four qubit is $|\widetilde{0}\rangle_i|\widetilde{0}\rangle_j|\widetilde{0}\rangle_k|\widetilde{0}\rangle_l$. After the impingement of the h polarized single photon on the beam splitter BS and through the phase shifter PS, the state of the whole system is $(|h\rangle_1 + |h\rangle_2)/\sqrt{2} \otimes |\widetilde{0}\rangle_i|\widetilde{0}\rangle_j|\widetilde{0}\rangle_k|\widetilde{0}\rangle_l$. We perform the operation $U_{\rm CPF}$ on the atom pairs in each cavity one by one at appropriate times with respect to the arrival of the photon at each cavity. Then we reach $\frac{1}{\sqrt{2}}(|h\rangle_1|\widetilde{0}\rangle_i|\widetilde{0}\rangle_j|\widetilde{0}\rangle_k|\widetilde{0}\rangle_l + |h\rangle_2|\widetilde{1}\rangle_i|\widetilde{1}\rangle_j|\widetilde{1}\rangle_k|\widetilde{1}\rangle_l)$, after the photon passes a 45° tilted half-wave plate (HWP 45°), a PBS, and then a P_{45}, the state will eventually become $\frac{(|h\rangle + |v\rangle)}{\sqrt{2}} \otimes \frac{1}{\sqrt{2}}(|\widetilde{0}\rangle_i|\widetilde{0}\rangle_j|\widetilde{0}\rangle_k|\widetilde{0}\rangle_l + |\widetilde{1}\rangle_i|\widetilde{1}\rangle_j|\widetilde{1}\rangle_k|\widetilde{1}\rangle_l)$. HWP 45°, with the axis by 45° with respect to the horizontal direction, rotate the photon polarization as $|h\rangle \leftrightarrow |v\rangle$. P_{45} is a 45° polarizer projecting the polarization $(|h\rangle + |v\rangle)/\sqrt{2}$. Therefore, by detecting a photon at detector D, we know with certainty that the logical four-qubit GHZ state has been generated. Obviously, this method of preparing a four-qubit GHZ state can be theoretically generalized to many-logical-qubit case just by adding more cavities with atomic pairs inside.

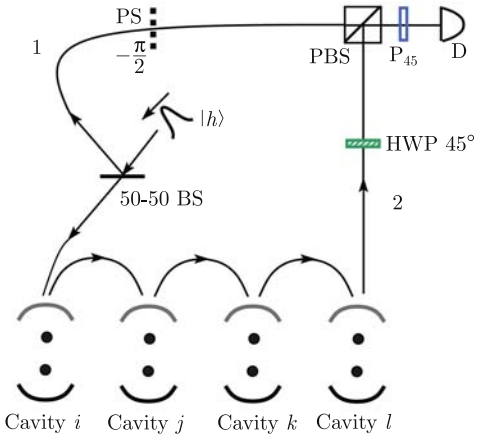

Fig. 2 Schematic setup for generating four-qubit GHZ state, BS is a 50-50 beam splitter, PS is a phase shifter with the shifted phase angle $-\pi/2$, PBS is a polarizing beam splitter, HWP 45° rotates the photon polarization as $|h\rangle \leftrightarrow |v\rangle$, D means a detector, and the optical paths 1 and 2 must be well designed for achieving good interference at PBS.

$$
\begin{aligned}
&|h\rangle \otimes |\widetilde{0}\rangle_i|\widetilde{0}\rangle_j|\widetilde{0}\rangle_k|\widetilde{0}\rangle_l \\
&\xrightarrow{\rm BS} (|h\rangle_1 + |h\rangle_2)/\sqrt{2} \otimes |\widetilde{0}\rangle_i|\widetilde{0}\rangle_j|\widetilde{0}\rangle_k|\widetilde{0}\rangle_l \\
&\xrightarrow{U_{\rm CPF}} \frac{1}{\sqrt{2}}(|h\rangle_1|\widetilde{0}\rangle_i|\widetilde{0}\rangle_j|\widetilde{0}\rangle_k|\widetilde{0}\rangle_l + |h\rangle_2|\widetilde{1}\rangle_i|\widetilde{1}\rangle_j|\widetilde{1}\rangle_k|\widetilde{1}\rangle_l) \\
&\xrightarrow{\text{HWP 45°}} \frac{1}{\sqrt{2}}(|h\rangle_1|\widetilde{0}\rangle_i|\widetilde{0}\rangle_j|\widetilde{0}\rangle_k|\widetilde{0}\rangle_l + |v\rangle_2|\widetilde{1}\rangle_i|\widetilde{1}\rangle_j|\widetilde{1}\rangle_k|\widetilde{1}\rangle_l) \\
&\xrightarrow{\text{PBS, P}_{45}} \frac{(|h\rangle + |v\rangle)}{\sqrt{2}} \otimes \frac{1}{\sqrt{2}}(|\widetilde{0}\rangle_i|\widetilde{0}\rangle_j|\widetilde{0}\rangle_k|\widetilde{0}\rangle_l \\
&\quad + |\widetilde{1}\rangle_i|\widetilde{1}\rangle_j|\widetilde{1}\rangle_k|\widetilde{1}\rangle_l) \qquad (4)
\end{aligned}
$$

In order to generate a GHZ state, we have to first design a controlled flip gate $\widetilde{X}$ between the photon and

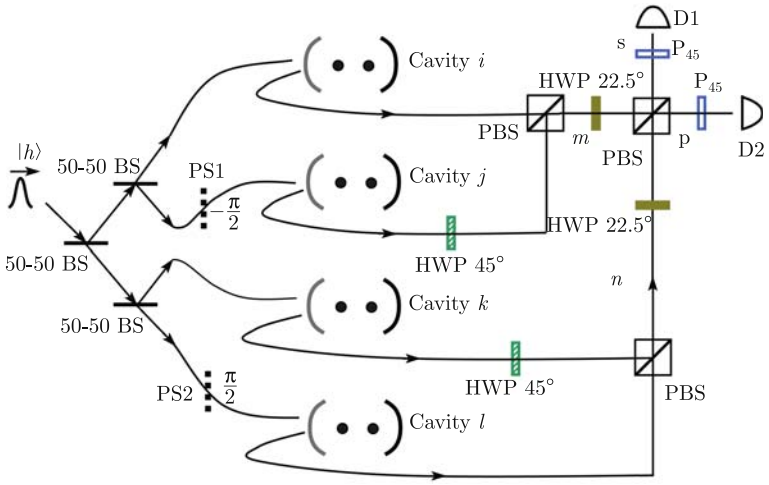

Fig. 3 Schematic setup for generating four-qubit W state, where each cavity confines two atoms, HWP 45° makes $|h\rangle \leftrightarrow |v\rangle$ and HWP 22.5° function as Hadamard gates to single photon. P_{45} means a 45° polarizer projecting the polarization to be $(|h\rangle+|v\rangle)/\sqrt{2}$. PS1 and PS2 are phase shifters with the shifted phase labeled nearby. The optical paths i, j, k, l, m and n must be well designed to achieve good interference at PBS.

the logical qubit, which functions that if there is a photon reflected by the cavity, then $|\widetilde{0}\rangle$ flips to $|\widetilde{1}\rangle$, and if there is no photon reflected, the quantum state remains unchanged. That is, a flip operation on the logic-qubit inside the cavity i, i.e., $\widetilde{X} = C^{2,1}_{\rm NOT} H_2 U_{\rm CPF} H_2 C^{2,1}_{\rm NOT}$ whose function is to flip the logic-qubit $|\widetilde{0}\rangle \leftrightarrow |\widetilde{1}\rangle$.

The schematic setup for generating a W state is shown in Fig. 3, where all the qubits are initially in the state $|\widetilde{0}\rangle_i|\widetilde{0}\rangle_j|\widetilde{0}\rangle_k|\widetilde{0}\rangle_l$ too. A single photon pulse with h polarization after passing three 50/50 beam splitters (BS), two phase shifters PS1 and PS2, have four possible outputs 1−4, each with 1/4 probability, that is, $\frac{1}{2}(|h\rangle_i + |h\rangle_j + |h\rangle_k + |h\rangle_l) \otimes |\widetilde{0}\rangle_i|\widetilde{0}\rangle_j|\widetilde{0}\rangle_k|\widetilde{0}\rangle_l$.

We do not know which path the photon goes through. However, we do the operations in $\widetilde{X}$ on each atomic pair at the appropriate time with respect to the arrival of the photon at the cavity. The key point is, if the photon comes out in the output i, then the logical qubit in cavity i will be flipped. So we get $\frac{1}{2}(|h\rangle_i|\widetilde{1}\rangle_i|\widetilde{0}\rangle_j|\widetilde{0}\rangle_k|\widetilde{0}\rangle_l + |h\rangle_j|\widetilde{0}\rangle_i|\widetilde{1}\rangle_j|\widetilde{0}\rangle_k|\widetilde{0}\rangle_l + |h\rangle_k|\widetilde{0}\rangle_i|\widetilde{0}\rangle_j|\widetilde{1}\rangle_k|\widetilde{0}\rangle_l + |h\rangle_l|\widetilde{0}\rangle_i|\widetilde{0}\rangle_j|\widetilde{0}\rangle_k|\widetilde{1}\rangle_l)$. After the photon reflection from the cavities, we combine the four paths into two paths: $\frac{1}{2}(|h\rangle_m|\widetilde{1}\rangle_i|\widetilde{0}\rangle_j|\widetilde{0}\rangle_k|\widetilde{0}\rangle_l + |v\rangle_m|\widetilde{0}\rangle_i|\widetilde{1}\rangle_j|\widetilde{0}\rangle_k|\widetilde{0}\rangle_l + |v\rangle_n|\widetilde{0}\rangle_i|\widetilde{0}\rangle_j|\widetilde{1}\rangle_k|\widetilde{0}\rangle_l + |h\rangle_n|\widetilde{0}\rangle_i|\widetilde{0}\rangle_j|\widetilde{0}\rangle_k|\widetilde{1}\rangle_l)$. At the output ports, we make measurement on the photon state with photon detectors D1 and D2, and the click of the detectors D1 and D2 correspond to the quantum state of the atom pairs $\frac{1}{2}(|\widetilde{1}\rangle_i|\widetilde{0}\rangle_j|\widetilde{0}\rangle_k|\widetilde{0}\rangle_l - |\widetilde{0}\rangle_i|\widetilde{1}\rangle_j|\widetilde{0}\rangle_k|\widetilde{0}\rangle_l + |\widetilde{0}\rangle_i|\widetilde{0}\rangle_j|\widetilde{1}\rangle_k|\widetilde{0}\rangle_l + |\widetilde{0}\rangle_i|\widetilde{0}\rangle_j|\widetilde{0}\rangle_k|\widetilde{1}\rangle_l)$ and $\frac{1}{2}(|\widetilde{1}\rangle_i|\widetilde{0}\rangle_j|\widetilde{0}\rangle_k|\widetilde{0}\rangle_l + |\widetilde{0}\rangle_i|\widetilde{1}\rangle_j|\widetilde{0}\rangle_k|\widetilde{0}\rangle_l - |\widetilde{0}\rangle_i|\widetilde{0}\rangle_j|\widetilde{1}\rangle_k|\widetilde{0}\rangle_l + |\widetilde{0}\rangle_i|\widetilde{0}\rangle_j|\widetilde{0}\rangle_k|\widetilde{1}\rangle_l)$, respectively.

The whole process can be summarized as follows:

$$
\begin{aligned}
&|h\rangle \otimes |\widetilde{0}\rangle_i|\widetilde{0}\rangle_j|\widetilde{0}\rangle_k|\widetilde{0}\rangle_l \\
\xrightarrow{\rm BS}\ &\frac{1}{2}(|h\rangle_i + |h\rangle_j + |h\rangle_k + |h\rangle_l) \\
&\otimes|\widetilde{0}\rangle_i|\widetilde{0}\rangle_j|\widetilde{0}\rangle_k|\widetilde{0}\rangle_l \\
\xrightarrow{\widetilde{X}}\ &\frac{1}{2}(|h\rangle_i|\widetilde{1}\rangle_i|\widetilde{0}\rangle_j|\widetilde{0}\rangle_k|\widetilde{0}\rangle_l \\
&+|h\rangle_j|\widetilde{0}\rangle_i|\widetilde{1}\rangle_j|\widetilde{0}\rangle_k|\widetilde{0}\rangle_l \\
&+|h\rangle_k|\widetilde{0}\rangle_i|\widetilde{0}\rangle_j|\widetilde{1}\rangle_k|\widetilde{0}\rangle_l \\
&+|h\rangle_l|\widetilde{0}\rangle_i|\widetilde{0}\rangle_j|\widetilde{0}\rangle_k|\widetilde{1}\rangle_l) \\
\xrightarrow{\text{HWP45°, PBS}}\ &\frac{1}{2}(|h\rangle_m|\widetilde{1}\rangle_i|\widetilde{0}\rangle_j|\widetilde{0}\rangle_k|\widetilde{0}\rangle_l \\
&+|v\rangle_m|\widetilde{0}\rangle_i|\widetilde{1}\rangle_j|\widetilde{0}\rangle_k|\widetilde{0}\rangle_l \\
&+|v\rangle_n|\widetilde{0}\rangle_i|\widetilde{0}\rangle_j|\widetilde{1}\rangle_k|\widetilde{0}\rangle_l \\
&+|h\rangle_n|\widetilde{0}\rangle_i|\widetilde{0}\rangle_j|\widetilde{0}\rangle_k|\widetilde{1}\rangle_l) \\
\xrightarrow{\text{HWP 22.5°,PBS,P}_{45}}\ &\frac{1}{4}\big[(|h\rangle_p + |v\rangle_p)(|\widetilde{1}\rangle_i|\widetilde{0}\rangle_j|\widetilde{0}\rangle_k|\widetilde{0}\rangle_l \\
&+|\widetilde{0}\rangle_i|\widetilde{1}\rangle_j|\widetilde{0}\rangle_k|\widetilde{0}\rangle_l - |\widetilde{0}\rangle_i|\widetilde{0}\rangle_j|\widetilde{1}\rangle_k|\widetilde{0}\rangle_l \\
&+|\widetilde{0}\rangle_i|\widetilde{0}\rangle_j|\widetilde{0}\rangle_k|\widetilde{1}\rangle_l) \\
&+(|h\rangle_s + |v\rangle_s)(|\widetilde{1}\rangle_i|\widetilde{0}\rangle_j|\widetilde{0}\rangle_k|\widetilde{0}\rangle_l \\
&-|\widetilde{0}\rangle_i|\widetilde{1}\rangle_j|\widetilde{0}\rangle_k|\widetilde{0}\rangle_l + |\widetilde{0}\rangle_i|\widetilde{0}\rangle_j|\widetilde{1}\rangle_k|\widetilde{0}\rangle_l \\
&+|\widetilde{0}\rangle_i|\widetilde{0}\rangle_j|\widetilde{0}\rangle_k|\widetilde{1}\rangle_l)\big] \\
\xrightarrow{\rm D}\ &{\rm D1}: \frac{1}{2}(|\widetilde{1}\rangle_i|\widetilde{0}\rangle_j|\widetilde{0}\rangle_k|\widetilde{0}\rangle_l \\
&-|\widetilde{0}\rangle_i|\widetilde{1}\rangle_j|\widetilde{0}\rangle_k|\widetilde{0}\rangle_l + |\widetilde{0}\rangle_i|\widetilde{0}\rangle_j|\widetilde{1}\rangle_k|\widetilde{0}\rangle_l \\
&+|\widetilde{0}\rangle_i|\widetilde{0}\rangle_j|\widetilde{0}\rangle_k|\widetilde{1}\rangle_l) \\
&{\rm D2}: \frac{1}{2}(|\widetilde{1}\rangle_i|\widetilde{0}\rangle_j|\widetilde{0}\rangle_k|\widetilde{0}\rangle_l \\
&+|\widetilde{0}\rangle_i|\widetilde{1}\rangle_j|\widetilde{0}\rangle_k|\widetilde{0}\rangle_l - |\widetilde{0}\rangle_i|\widetilde{0}\rangle_j|\widetilde{1}\rangle_k|\widetilde{0}\rangle_l \\
&+|\widetilde{0}\rangle_i|\widetilde{0}\rangle_j|\widetilde{0}\rangle_k|\widetilde{1}\rangle_l) \qquad (5)
\end{aligned}
$$

To get the standard W state, we further operate to make $-|\widetilde{1}\rangle_j$ be $|\widetilde{1}\rangle_j$ and $-|\widetilde{1}\rangle_k$ be $|\widetilde{1}\rangle_k$, by reflecting an auxiliary single-photon with h polarization to the cavity i, i.e., $\sigma^1_{x,1} U_{\rm CPF} \sigma^1_{x,i}$, with $\sigma^1_{x,1}$ the NOT gate performed on the 1th atom in the ith cavity.

Cluster state is a special kind of entangled resource processed in one-way condition and only needs a sequence of one-qubit projective measurements [23, 24]. To generate a cluster state, one should first initialize each logical qubit in superposition state $|\widetilde{+}\rangle_i = (|\widetilde{0}\rangle_i + |\widetilde{1}\rangle_i)1/\sqrt{2}$, and then perform controlled phase gates on nearest-neighbor qubits. The superposition state can be made from the state $|\widetilde{0}\rangle_i$ by a photon scattering as follows:

$$
\begin{aligned}
&\frac{1}{\sqrt{2}}(|h\rangle + |v\rangle) \otimes |\widetilde{0}\rangle_i \\
\xrightarrow{\rm PBS(}U_{\rm CPF}{\rm)}\ &\frac{1}{\sqrt{2}}(|h\rangle|\widetilde{1}\rangle_i + |v\rangle|\widetilde{0}\rangle_i) \\
\xrightarrow{\rm P_{45}}\ &\frac{1}{\sqrt{2}}(|h\rangle + |v\rangle) \otimes \frac{1}{\sqrt{2}}(|\widetilde{1}\rangle_i + |\widetilde{0}\rangle_i) \qquad (6)
\end{aligned}
$$

where the PBS is used to reflect the photons v component as plotted in Fig. 4. As a result, the detection of a photon makes sure that the state $|\widetilde{+}\rangle_i$ has been successfully generated. The schematic setup in Fig. 4 is for implementing nonlocal controlled phase gate in the DFSs, where some NOT gates on individual atoms are not plotted in the figure. We assume that the input photon is initially in the state $(|h\rangle + |v\rangle)/\sqrt{2}$ and the two

remote qubits in arbitrary state $\alpha_{00}|\widetilde{0}\rangle_i|\widetilde{0}\rangle_j+\alpha_{01}|\widetilde{0}\rangle_i|\widetilde{1}\rangle_j+\alpha_{10}|\widetilde{1}\rangle_i|\widetilde{0}\rangle_j+\alpha_{11}|\widetilde{1}\rangle_i|\widetilde{1}\rangle_j$. And the corresponding result is

$$\begin{aligned}
&\xrightarrow{\sigma^2_{x,1}U_{\rm CPF}\sigma^2_{x,i}} \frac{1}{\sqrt{2}}\big[\alpha_{00}(-|h\rangle+|v\rangle)|\widetilde{0}\rangle_i|\widetilde{0}\rangle_j\\
&\quad+\alpha_{01}(-|h\rangle+|v\rangle)|\widetilde{0}\rangle_i|\widetilde{1}\rangle_j\\
&\quad+\alpha_{10}(|h\rangle+|v\rangle)|\widetilde{1}\rangle_i|\widetilde{0}\rangle_j\\
&\quad+\alpha_{11}(|h\rangle+|v\rangle)|\widetilde{1}\rangle_i|\widetilde{1}\rangle_j\big]\\
&\xrightarrow{\text{HWP 45°, HWP 22.5°}} \alpha_{00}|v\rangle|\widetilde{0}\rangle_i|\widetilde{0}\rangle_j+\alpha_{01}|v\rangle|\widetilde{0}\rangle_i|\widetilde{1}\rangle_j\\
&\quad+\alpha_{10}|h\rangle|\widetilde{1}\rangle_i|\widetilde{0}\rangle_j\\
&\quad+\alpha_{11}|h\rangle|\widetilde{1}\rangle_i|\widetilde{1}\rangle_j\\
&\xrightarrow{\sigma^2_{x,1}U_{\rm CPF}\sigma^2_{x,i},{\rm P}_{45}} \frac{1}{\sqrt{2}}(\alpha_{00}|\widetilde{0}\rangle_i|\widetilde{0}\rangle_j+\alpha_{01}|\widetilde{0}\rangle_i|\widetilde{1}\rangle_j\\
&\quad+\alpha_{10}|\widetilde{1}\rangle_i|\widetilde{0}\rangle_j+\alpha_{11}|\widetilde{1}\rangle_i|\widetilde{1}\rangle_j) \qquad (7)
\end{aligned}$$

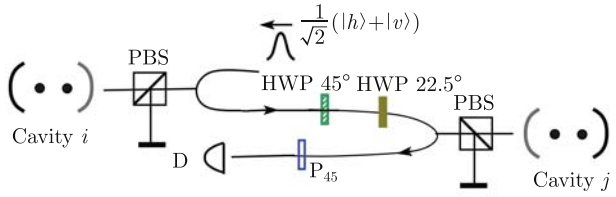

Fig. 4 Schematic setup for implementing nonlocal controlled phase gate in the DFSs.

Therefore, by detecting the photon, we know with certainty that the controlled phase gate has been successfully implemented. Provided that the initial state $|\widetilde{+}\rangle_i|\widetilde{+}\rangle_j|\widetilde{+}\rangle_k|\widetilde{+}\rangle_l$ has been prepared, the performance of controlled phase gates between logical qubits k and l, between logical qubits j and k, and between logical qubits i and j, can transform the initial state into a one-dimensional four-qubit cluster state. Our idea is in principle extendable to many-qubit cluster states.

3 Information transfer of quantum states encoded in DFS

We hope the physical arrangement in our scheme is capable of carrying out a variety of QIP tasks without a significant modification of the setup itself. For example, for the cavity QED system, we hope it can do as much quantum information work as possible, initialization of entangled states, quantum state transfer, quantum search algorithms, even quantum computation, under the similar setup condition. Compatible QIP is one direction in which researchers should develop. In our scheme for qubits encoded in pairs of atoms in DFS, in this section, we can show how to implement transfer and teleportation of quantum states in DFS [29].

The information transfer in our scheme can not only protect quantum information from some decoherence, but also reduce the experimental difficulty compared to the previous schemes [30]. Furthermore, in our scheme, each node of the quantum network in DFS has an individual input port for photons to complete necessary operations, and different operational results can be distinguished by detecting output photons.

To carry out a quantum transfer and a teleportation in the DFS, we need to construct a Hadamard operation $\widetilde{H}$ on the single-logic qubit and a conditional gate operation on the two-logic qubit. The $\widetilde{H}$ operation is shown in Fig. 5 for the logic-qubit at arbitrary node i (or, say, cavity i). TR is a device which can be controlled exactly as needed to transmit or reflect a photon, and the switching-time sequences of TR1 and TR2 are also given in Fig. 5.

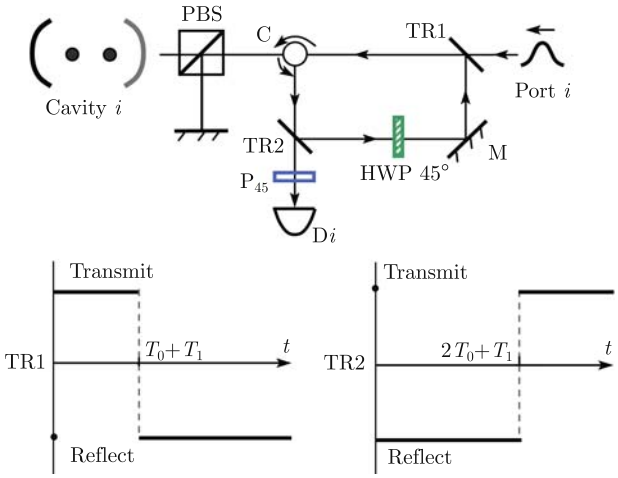

Fig. 5 Schematic setup for a single-logic-qubit $\widetilde{H}$ operation and time control sequence of TR1 and TR2. Di is a detector, C is a circulator. TR can be controlled exactly as needed to transmit or to reflect a photon. The single-photon pulse's path for $\widetilde{H}$ is port i-TR1-C-PBS-Cavity-PBS-C-TR2-HWP 45°-M-TR1-C-PBS-Cavity-PBS-C-TR2-P_{45}-Di. The states of TR1 and TR2 can be controlled accurately by computer. T_0 is the time for single-photon pulse process TR1-C-PBS-Cavity-PBS-C-TR2, while T_1 is the time for TR2-HWP 45°-M-TR1.

Assume that the state of the logic-qubit in cavity i is $|\widetilde{1}\rangle$. The $\widetilde{H}$ operation can be performed by following four steps:

(1) A single-photon pulse in state $(|h\rangle+|v\rangle)/\sqrt{2}$ is imported from port i. It passes through TR1 and C, and then reaches the PBS and the cavity i. Meanwhile, we perform a flip operation on the logic-qubit inside the cavity i, i.e., $\widetilde{X}=C^{2,1}_{\rm NOT}H_2U_{\rm CPF}H_2C^{2,1}_{\rm NOT}$ whose function is to flip the logic-qubit $|\widetilde{0}\rangle\leftrightarrow|\widetilde{1}\rangle$, and thereby the state becomes $(|h\rangle|\widetilde{0}\rangle+|v\rangle|\widetilde{1}\rangle)/\sqrt{2}$ after the photon pulse comes

back from the cavity i and the PBS.

(2) Reflected by TR2, the photon pulse goes through HWP 45°, yielding the state $(|v\rangle|\widetilde{0}\rangle + |h\rangle|\widetilde{1}\rangle)/\sqrt{2}$.

(3) After being reflected by M and TR1, the single-photon pulse arrives at PBS again. We need two NOT operations on atom 1, one before and another after the photon pulse is reflected by the cavity, i.e., the operation sequence $\sigma_x^1 U_{\rm CFP}\sigma_x^1$. So we get to the state $(|v\rangle|\widetilde{0}\rangle - |h\rangle|\widetilde{1}\rangle)/\sqrt{2}$.

(4) Finally, when the single-photon pulse passes TR2 and $\rm P_{45}$, the photon is detected by Di, and thereby the logic-qubit inside the cavity i is left in the state $(|\widetilde{0}\rangle - |\widetilde{1}\rangle)/\sqrt{2}$.

The operation process above can be shown more specifically as follows:

$$\begin{aligned}\frac{|h\rangle+|v\rangle}{\sqrt{2}}|\widetilde{1}\rangle &\xrightarrow{\widetilde{X}} \frac{1}{\sqrt{2}}(|h\rangle|\widetilde{0}\rangle + |v\rangle|\widetilde{1}\rangle)\\ &\xrightarrow{\text{HWP } 45^\circ} \frac{1}{\sqrt{2}}(|v\rangle|\widetilde{0}\rangle + |h\rangle|\widetilde{1}\rangle)\\ &\xrightarrow{\sigma_x^1 U_{\rm CFP}\sigma_x^1} \frac{1}{\sqrt{2}}(|v\rangle|\widetilde{0}\rangle - |h\rangle|\widetilde{1}\rangle)\\ &\xrightarrow{\rm P_{45}} \frac{|h\rangle+|v\rangle}{\sqrt{2}}\frac{1}{\sqrt{2}}(|\widetilde{0}\rangle - |\widetilde{1}\rangle) \qquad (8)\end{aligned}$$

So a click of Di means the success of the Hadamard gate on the logic qubit. Otherwise, we have to repeat the above steps from the very beginning with the single photon input and initial atomic state preparation. It is easy to check that Fig. 5 also works for $|\widetilde{0}\rangle$ to be $(|\widetilde{0}\rangle + |\widetilde{1}\rangle)1/\sqrt{2}$. Compared with the previous operation of a single-logic-qubit Hadamard gate [31], our proposal needs neither the ancilla system to store information nor the optical lattices to transfer atoms synchronously across the cavity.

To ensure the success of the above operations, we require the switching time sequences of TR to be implemented accurately. Actually, in addition to the time control sequences of TR1 and TR2 designed in Fig. 5, we have an alternative. Take TR1 for instance: Once the single-photon pulse from port i has gone through TR1, we change the transmitting state of the TR1 into reflecting state without waiting for the time $T_0 + T_1$. The switching-time sequence designed for $\widetilde{H}$ is general for arbitrary states of the single-logic qubit.

A two-node controlled phase gate for logic-qubits encoded in a DFS, without using the entangle photon pairs as in Ref. [32], can be implemented with the aid of an additional channel shown by dashed gray lines in Fig. 6. $\widetilde{U}_{\text{C-Z}}^{i,j}$ is a controlled Z (C-Z) phase- flip gate with subscripts i and j indicating the control and target logic-qubits in cavities i and j, respectively. Assume that the two logic-qubits are in superposition state, $a|\widetilde{0}\rangle_i|\widetilde{0}\rangle_j + b|\widetilde{0}\rangle_i|\widetilde{1}\rangle_j + c|\widetilde{1}\rangle_i|\widetilde{0}\rangle_j + d|\widetilde{1}\rangle_i|\widetilde{1}\rangle_j$, where a, b, c and d are normalized constants. The $\widetilde{U}_{\text{C-Z}}^{i,j}$ operation is completed by the following three steps:

(1) A single-photon pulse in state $(|h\rangle + |v\rangle)/\sqrt{2}$ is input from the port i, passes through PBS, and reaches the cavity i. We need to perform the following operations $\sigma_{x,i}^2 U_{\rm CPF}\sigma_{x,i}^2$, i.e., σ_x operation on the atom 2 in cavity i before and after the single-photon pulse is reflected by the cavity i.

(2) Because of reflection of TR2, the single-photon pulse passes through HWP 45° and goes into the additional channel connected to the node j.

(3) After going through HWP 22.5° and reflected by TR3*, the single-photon pulse arrives at the PBS and then the cavity j. As previously, we have to perform $\sigma_{x,j}^1 U_{\rm CPF}\sigma_{x,j}^1$, i.e., the σ_x operation, on the atom 1 in the cavity j before and after the single-photon pulse is reflected by the cavity j. Then the single-photon pulse goes through $\rm P_{45}$ and would be detected by Dj.

The $\widetilde{U}_{\text{C-Z}}^{i,j}$ operation process above can be shown step by step as:

$$\begin{aligned}&\frac{1}{\sqrt{2}}(|h\rangle+|v\rangle)\otimes(a|\widetilde{0}\rangle_i|\widetilde{0}\rangle_j + b|\widetilde{0}\rangle_i|\widetilde{1}\rangle_j\\ &+c|\widetilde{1}\rangle_i|\widetilde{0}\rangle_j + d|\widetilde{1}\rangle_i|\widetilde{1}\rangle_j)\\ &\xrightarrow{\sigma_{x,i}^2 U_{\rm CFP}\sigma_{x,i}^2} \frac{1}{\sqrt{2}}[a(-|h\rangle+|v\rangle)|\widetilde{0}\rangle_i|\widetilde{0}\rangle_j\\ &\qquad +b(-|h\rangle+|v\rangle)|\widetilde{0}\rangle_i|\widetilde{1}\rangle_j\\ &\qquad +c(|h\rangle+|v\rangle)|\widetilde{1}\rangle_i|\widetilde{0}\rangle_j\\ &\qquad +d(|h\rangle+|v\rangle)|\widetilde{1}\rangle_i|\widetilde{1}\rangle_j] \qquad (9)\\ &\xrightarrow{\text{HWP } 45^\circ,\ \text{HWP } 22.5^\circ} a|v\rangle|\widetilde{0}\rangle_i|\widetilde{0}\rangle_j\\ &\qquad +b|v\rangle|\widetilde{0}\rangle_i|\widetilde{1}\rangle_j + c|h\rangle|\widetilde{1}\rangle_i|\widetilde{0}\rangle_j\\ &\qquad +d|h\rangle|\widetilde{1}\rangle_i|\widetilde{1}\rangle_j\\ &\xrightarrow{\sigma_{x,j}^1 U_{\rm CFP}\sigma_{x,j}^1,\rm P_{45}} \frac{1}{\sqrt{2}}(|h\rangle+|v\rangle)\otimes(a|\widetilde{0}\rangle_i|\widetilde{0}\rangle_j\\ &\qquad +b|\widetilde{0}\rangle_i|\widetilde{1}\rangle_j + c|\widetilde{1}\rangle_i|\widetilde{0}\rangle_j - d|\widetilde{1}\rangle_i|\widetilde{1}\rangle_j)\end{aligned}$$

If we get a click of Dj, the $\widetilde{U}_{\text{C-Z}}^{i,j}$ operation succeeds. The silence of Dj means failure and we must repeat the above steps from the very beginning. Considering the symmetric operation for the two qubits gate, the $\widetilde{U}_{\text{C-Z}}^{j,i}$ operation can be done by a similar process to Eq. (9), where the single-photon pulse is input from port j, as shown in Fig. 6. The corresponding controlled-NOT(CNOT) operation for the logic qubits in a DFS is given by $\widetilde{C}_{\rm NOT}^{i,j} = \widetilde{H}_j \otimes \widetilde{U}_{\text{C-Z}}^{i,j} \otimes \widetilde{H}_j$ and $\widetilde{C}_{\rm NOT}^{j,i} = \widetilde{H}_i \otimes \widetilde{U}_{\text{C-Z}}^{j,i} \otimes$

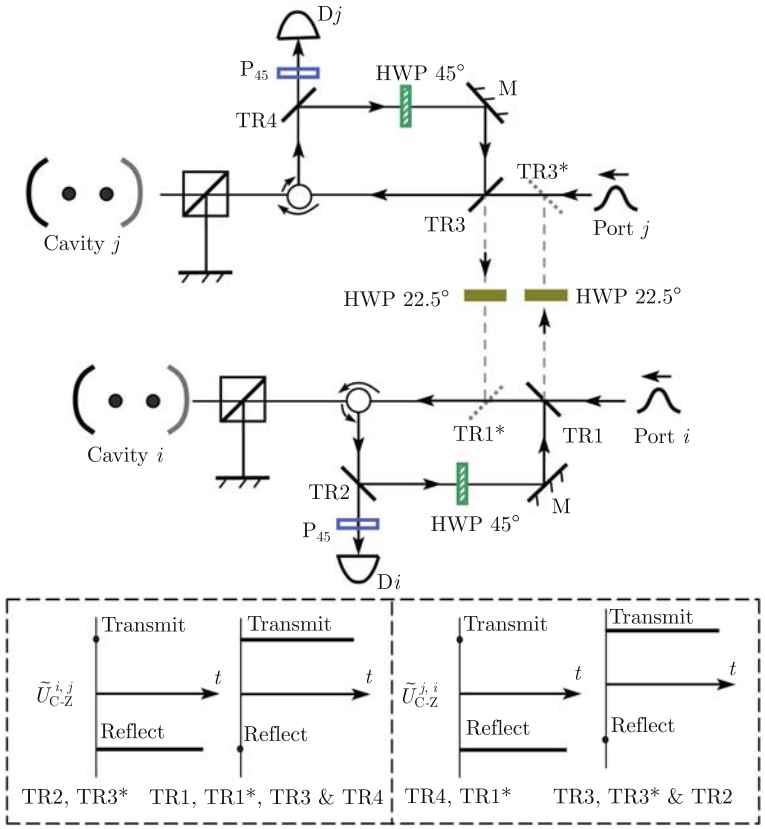

Fig. 6 Schematic setup for two logic-qubit conditional phase gate $\widetilde{U}^{i,j}_{\text{C-Z}}$ ($\widetilde{U}^{j,i}_{\text{C-Z}}$) which uses the additional channel shown by dashed gray lines. The single-photon pulse's path for $\widetilde{U}^{i,j}_{\text{C-Z}}$ ($\widetilde{U}^{j,i}_{\text{C-Z}}$) is: port i-TR1-TR1*-C-PBS-Cavity i-PBS-C-TR2-HWP 45°-M-TR1-HWP 22.5°-TR3*-TR3 -C-PBS-Cavity j-PBS-C-TR4-P_{45}-Dj (port j-TR3*-TR3-C-PBS-Cavity j-PBS-C-TR4-HWP 45°-M-TR3-HWP 22.5°-TR1*-C- PBS-Cavity i-PBS-C-TR2-P_{45}-Di). Ulike $\widetilde{H}$, the TRs remain unchanged during the conditional phase gating.

$\widetilde{H}_i$. It should be mentioned that, the TR1* (or TR3* for node j), whose function is to connect spatially separated nodes, has no action during the single-logic-qubit Hadamard operation. So we can keep them always on in transmitting state during the time the $\widetilde{H}$ operation is carried out in individual nodes.

The transfer of information in a quantum network is an important subject for quantum information processing [30]. Based on the operations investigated above, we realize below the information exchange between the ith logic-qubit $\alpha_i|\widetilde{0}\rangle + \beta_i|\widetilde{1}\rangle$ and the jth logic-qubit $\alpha_j|\widetilde{0}\rangle + \beta_j|\widetilde{1}\rangle$, using the following single-photon pulse sequence:

$$\widetilde{U}^{i,j}_{\text{SWAP}} = \widetilde{C}^{i,j}_{\text{NOT}}\widetilde{C}^{j,i}_{\text{NOT}}\widetilde{C}^{i,j}_{\text{NOT}} \tag{10}$$

The corresponding process reads $(\alpha_i|\widetilde{0}\rangle + \beta_i|\widetilde{1}\rangle)(\alpha_j|\widetilde{0}\rangle + \beta_j|\widetilde{1}\rangle) \rightarrow (\alpha_j|\widetilde{0}\rangle + \beta_j|\widetilde{1}\rangle)(\alpha_i|\widetilde{0}\rangle + \beta_i|\widetilde{1}\rangle)$. Compared with previous work [30], we do not need the special laser pulses with time-dependent Rabi frequency and laser phases to excite a time-symmetric wave packet of the photon from the sending node to the receiving node. In addition, we do not require a transfer channel made using auxiliary entangled photon pairs. More importantly, compared to Ref. [30], our logic-qubits are encoded in DFS which is robust to collective dephasing error.

Now we turn to a proposal for quantum state teleportation [33] for the logic qubits described above. Assume that we have three logic-qubits in states $|\widetilde{\Psi}\rangle_i$, $|\widetilde{\Psi}\rangle_j$ and $|\widetilde{\Psi}\rangle_k$, respectively, with the former two belonging to Alice and the third to Bob. $|\widetilde{\Psi}\rangle_i = \alpha|\widetilde{0}\rangle + \beta|\widetilde{1}\rangle$ is an unknown state and would be teleported to Bob. First, teleportation need entanglement between Alice's second qubit $|\widetilde{\Psi}\rangle_j$ and Bob's qubit $|\widetilde{\Psi}\rangle_k$ in a Bell state. We take $|\widetilde{\Psi}\,\widetilde{\Psi}\rangle_{jk} = \dfrac{1}{\sqrt{2}}(|\widetilde{0}\rangle_j|\widetilde{0}\rangle_k + |\widetilde{1}\rangle_j|\widetilde{1}\rangle_k)$ for example. The Bell-style entanglement can be implemented by $\widetilde{H}$ and $\widetilde{C}_{\text{NOT}}$ operation for the initial state $|\widetilde{0}\rangle_j|\widetilde{0}\rangle_k$, i.e.,

$$\begin{aligned}|\widetilde{0}\rangle_j|\widetilde{0}\rangle_k &\xrightarrow{\widetilde{H}_j} \frac{1}{\sqrt{2}}(|\widetilde{0}\rangle_j + |\widetilde{1}\rangle_j)|\widetilde{0}\rangle_k \\ &\xrightarrow{\widetilde{C}^{j,k}_{\text{NOT}}} \frac{1}{\sqrt{2}}(|\widetilde{0}\rangle_j|\widetilde{0}\rangle_k + |\widetilde{1}\rangle_j|\widetilde{1}\rangle_k)\end{aligned} \tag{11}$$

The Bell state measurement in teleportation also uses

$\widetilde{H}$ and $\widetilde{C}_{\rm NOT}$ operations, i.e., a $\widetilde{C}^{i,j}_{\rm NOT}$ operation between $|\widetilde{\Psi}\rangle_i$ and $|\widetilde{\Psi}\rangle_j$ and an $\widetilde{H}_i$ operation to $|\widetilde{\Psi}\rangle_i$. As a result, we get the final state $|\widetilde{\Phi}\rangle = \frac{1}{2}[|\widetilde{0}\rangle_i|\widetilde{0}\rangle_j(\alpha|\widetilde{0}\rangle + \beta|\widetilde{1}\rangle)_k + |\widetilde{0}\rangle_i|\widetilde{1}\rangle_j(\alpha|\widetilde{1}\rangle + \beta|\widetilde{0}\rangle)_k + |\widetilde{1}\rangle_i|\widetilde{0}\rangle_j(\alpha|\widetilde{0}\rangle - \beta|\widetilde{1}\rangle)_k + |\widetilde{1}\rangle_i|\widetilde{1}\rangle_j(\alpha|\widetilde{1}\rangle - \beta|\widetilde{0}\rangle)_k]$. Following the operations shown in Table 1, we finish the teleportation of a quantum state from the logic-qubit i to the logic-qubit k.

Table 1 Bob's corresponding operations on the logic-qubit $|\widetilde{\Psi}\rangle_k$ after he has learned the measurement outcomes from Alice by a classical communication channel. $\sigma^1_{x,k}$ means σ_x operation on the atom 1 in cavity k. The $\widetilde{X}$ operation has been given in the text.

Alice's measurements	Bob's operations
$\|\widetilde{0}\rangle_i\|\widetilde{0}\rangle_j$	Nothing
$\|\widetilde{0}\rangle_i\|\widetilde{1}\rangle_j$	$\widetilde{X}$
$\|\widetilde{1}\rangle_i\|\widetilde{0}\rangle_j$	$\widetilde{Z} = \sigma^1_{x,k}U_{\rm CPF}\sigma^1_{x,k}$
$\|\widetilde{1}\rangle_i\|\widetilde{1}\rangle_j$	$\widetilde{Z}\widetilde{X}$

From the schematic setup in Fig. 6 and the operations presented above, we can learn that the single-logical-qubit Hadamard operation and the two-logical-qubit conditional operation are coexisting in our scheme and could work independently by controlling the transmitting or reflecting state of the connecting devices TR1* and TR3*. This is very important for scalability of the quantum network.

4 Two-qubit Grover search in DFS

The Grover search algorithm [34, 35] is an efficient quantum algorithm to look for items in an unsorted database. The efficiency of this algorithm has been tested experimentally in two-qubit cases by NMR [36, 37], by trapped ions [20] and by linear optics [38, 39]. In this section, we will briefly review the Grover search and the necessary operations. Then we discuss how to carry out these operations in our cavity-QED system, based on which the implementation of a two-qubit Grover search is made. We also discuss the compatibility and scalability of the present tailored scheme [40].

Grover search starts from a superposition state $|\Psi_0\rangle = (1/\sqrt{N})\sum_{x=0}^{N-1}|x\rangle$ $(x = 0, 1, \cdots, N-1)$, where each item has an equal probability to get picked. One search step (i.e., a query) includes two key operations [34, 35]: (i) inverting the amplitude of the marked state; and (ii) performing a diffusion transform D, i.e., inversion about the average state $|\Psi_0\rangle$ with $D_{ij} = 2/N$ for $i \neq j$ and $D_{ii} = -1 + 2/N$. If the target item is $|T\rangle$, then the operation in the step (i) results in a conditional phase gate $I_T = I - 2|T\rangle\langle T|$, where I is the $N \times N$ identity matrix. After $O(\sqrt{N})$ queries, the amplitude of the identified target will be amplified while the amplitudes of nontarget items are shrunk. Thus we get the target item by measurement with high probability.

The two-qubit Grover search has been proposed to be carried out in cavity QED [41, 42]. About the Grover search in DFS, a scheme with trapped ion pairs as qubits in DFS is proposed in Ref. [43]. QIP in DFS needs the efficient operations on encoded logic-qubits, $|\widetilde{0}\rangle$, $|\widetilde{1}\rangle$ and their arbitrary superposition. With regard to Grover search in DFS, the necessary logic-qubit operations are single-logic-qubit Hadamard gate $\widetilde{H}$ and two-logic-qubit controlled phase flip (CPF) gate $\widetilde{U}_{\rm CPF}$. Based on these basic operations, we will construct the diffusion transform operation $\widetilde{D}$ in DFS and different $\widetilde{U}_{\rm CPF}$ for different target items. Our scheme has the following favorable features in implementation of the Grover search:

(i) All correlative atom levels have the same qubit encoding.

(ii) Each logic-qubit (or, say, node in DFS) has individual input port for photons to complete necessary operations, and different operational results can be distinguished by detecting output photons.

(iii) The single-logic-qubit Hadamard operation and the two-logic-qubit conditional phase operation are coexisting in our scheme and could work independently by controlling the corresponding optic devices. This is helpful to extend our idea to the more-qubit Grover search.

(iv) Different $\widetilde{U}_{\rm CPF}$ and $\widetilde{D}$ for different target items have similar operations.

(v) More importantly, as collective dephasing errors are strongly suppressed in our design, we need no refocusing pulses for modification. This makes our implementation simplified although the DFS encoding seems to use more qubit resources.

(vi) Finally, we improve our previous scheme [29] to ensure the realistic expansion to N-qubit quantum network without the limit that it is only suitable to the two cavity connection case.

All the operations on the logic-qubit in our scheme is based on the two-atom controlled phase gate $U_{\rm CPF}$ completed by the cavity-assisted photon scattering. To manipulate a single logic-qubit in the DFS, Hadamard gate $\widetilde{H}$ on logic-qubit is very important. The integrated photon path for the $\widetilde{H}$ operation is shown in Fig. 7 for the logic-qubit at arbitrary node i (or, say, cavity i).

Assume that $|\widetilde{1}\rangle$ is the initial state of the logic-qubit in cavity i. The $\widetilde{H}$ operation can be completed by following steps. At the beginning, we import a $(|h\rangle + |v\rangle)/\sqrt{2}$ single-photon pulse from port i. The photon pulse will pass through TRi 1 and C, and then reach the polarizing beam splitter (PBS) and the cavity i. A flip operation

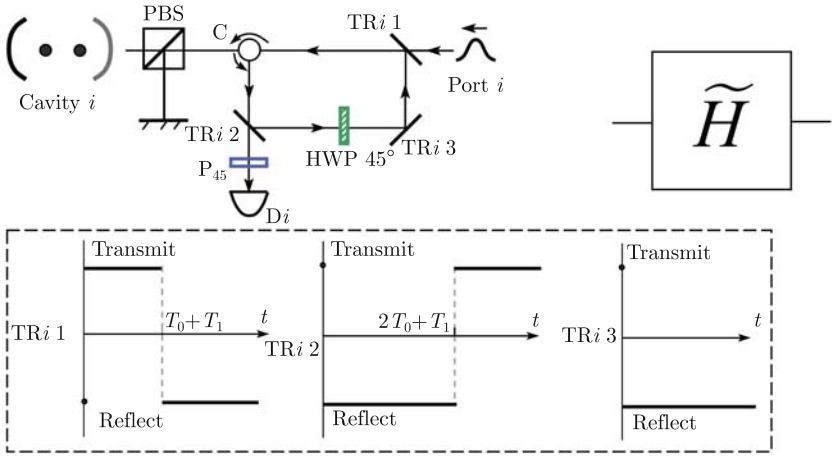

Fig. 7 Schematic setup for a single-logic-qubit $\widetilde{H}$ operation. Di is a detector, C is a circulator. HWP 45° rotates the photon polarization as $|h\rangle \leftrightarrow |v\rangle$. TR can be controlled exactly as needed to transmit or to reflect a photon. The single-photon pulse's path for $\widetilde{H}$ is port i -TRi 1-C-PBS-Cavity-PBS-C-TRi 2-HWP 45°-TRi 3-TRi 1-C-PBS-Cavity-PBS-C-TRi 2-P$_{45}$-Di. The states of TRi 1, TRi 2 and TRi 3 can be controlled accurately by computer. TRi stands for the TR belongs to node i. T_0 is the time for single-photon pulse process TRi 1-C-PBS-Cavity-PBS-C-TRi 2, while T_1 is the time for TRi 2-HWP 45°-TRi 3-TRi 1. For convenience of description below for Grover search, we denote the operation by a block $\widetilde{H}$.

on the logic-qubit inside the cavity i $\widetilde{X} = C_{\rm NOT}^{2,1} H_2 U_{\rm CPF} H_2 C_{\rm NOT}^{2,1}$ is needed to flip the logic-qubit $|\widetilde{0}\rangle \leftrightarrow |\widetilde{1}\rangle$ [20], during which the input photon is used to complete the operation $U_{\rm CPF}$ in $\widetilde{X}$. Subsequently, the state becomes $(|h\rangle|\widetilde{0}\rangle + |v\rangle|\widetilde{1}\rangle)/\sqrt{2}$ after the photon pulse returns from the cavity i and the PBS. Reflected by TRi 2, the photon pulse goes through HWP 22.5°, resulting in the state $(|v\rangle|\widetilde{0}\rangle + |h\rangle|\widetilde{1}\rangle)/\sqrt{2}$. After the single-photon pulse is reflected by M and TRi 1, it arrives at PBS again. Two NOT operations are needed on atom 1, one before and another after the photon pulse is reflected by the cavity, i.e., the operation sequence $\sigma_x^1 U_{\rm CPF} \sigma_x^1$. So we obtain the state $(|v\rangle|\widetilde{0}\rangle - |h\rangle|\widetilde{1}\rangle)/\sqrt{2}$. Finally, when it passes TRi 2 and P$_{45}$, the single photon pulse is detected by Di. Meanwhile the $\widetilde{H}$ operation is completed and the logic-qubit inside the cavity i is left in the state $(|\widetilde{0}\rangle - |\widetilde{1}\rangle)/\sqrt{2}$.

The operation process can be expressed in formula compendiously as follows:

$$\begin{aligned}
&\frac{|h\rangle+|v\rangle}{\sqrt{2}}|\widetilde{0}\rangle \xrightarrow{\widetilde{X}} \frac{1}{\sqrt{2}}(|h\rangle|\widetilde{1}\rangle + |v\rangle|\widetilde{0}\rangle) \\
&\quad \xrightarrow{\text{HWP } 45^\circ} \frac{1}{\sqrt{2}}(|v\rangle|\widetilde{1}\rangle + |h\rangle|\widetilde{0}\rangle) \\
&\quad \xrightarrow{\sigma_x^1 U_{\rm CPF} \sigma_x^1} \frac{1}{\sqrt{2}}(|v\rangle|\widetilde{1}\rangle + |h\rangle|\widetilde{0}\rangle) \\
&\quad \xrightarrow{\text{P}_{45}} \frac{|h\rangle+|v\rangle}{\sqrt{2}}\frac{1}{\sqrt{2}}(|\widetilde{1}\rangle + |\widetilde{0}\rangle) \qquad (12) \\
&\frac{|h\rangle+|v\rangle}{\sqrt{2}}|\widetilde{1}\rangle \xrightarrow{\widetilde{X}} \frac{1}{\sqrt{2}}(|h\rangle|\widetilde{0}\rangle + |v\rangle|\widetilde{1}\rangle) \\
&\quad \xrightarrow{\text{HWP } 45^\circ} \frac{1}{\sqrt{2}}(|v\rangle|\widetilde{0}\rangle + |h\rangle|\widetilde{1}\rangle) \\
&\quad \xrightarrow{\sigma_x^1 U_{\rm CPF} \sigma_x^1} \frac{1}{\sqrt{2}}(|v\rangle|\widetilde{0}\rangle - |h\rangle|\widetilde{1}\rangle) \\
&\quad \xrightarrow{\text{P}_{45}} \frac{|h\rangle+|v\rangle}{\sqrt{2}}\frac{1}{\sqrt{2}}(|\widetilde{0}\rangle - |\widetilde{1}\rangle) \qquad (13)
\end{aligned}$$

From the Fig. 7, we can find a click of Di meaning the success of the Hadamard gate on the logic qubit. Otherwise, we have to repeat the above steps from the very beginning with the single photon input and initial atomic state preparation. About the switching time sequences of TR, we give a brief illustration in Fig. 7 and we will give a detailed description related with operations in Grover search in the discussion part below.

We will focus more attention on all the two-qubit conditional phase gates on the logic-qubit, which is not present in the previous works. Two-logic-qubit conditional phase gate $\widetilde{U}_{\rm CPF}$, including four-phase flip gates $\widetilde{U}_{{\rm CPF}|\widetilde{0}\rangle|\widetilde{0}\rangle}$, $\widetilde{U}_{{\rm CPF}|\widetilde{0}\rangle|\widetilde{1}\rangle}$, $\widetilde{U}_{{\rm CPF}|\widetilde{1}\rangle|\widetilde{0}\rangle}$, and $\widetilde{U}_{{\rm CPF}|\widetilde{1}\rangle|\widetilde{1}\rangle}$ triggered by the condition that the two logic-qubits in the state $|\widetilde{0}\rangle|\widetilde{0}\rangle$, $|\widetilde{0}\rangle|\widetilde{1}\rangle$, $|\widetilde{1}\rangle|\widetilde{0}\rangle$ and $|\widetilde{1}\rangle|\widetilde{1}\rangle$, respectively, can be implemented with the aid of an additional channel shown by dashed gray lines in Fig. 8. Superscripts $c1$ and $c2$ in $\widetilde{U}_{\rm CPF}^{c_1,c_2}$ indicate that the logic-qubits need conditional phase operations in cavities $c_1 = i, j, k$ and $c_2 = i, j, k$ $(c_1 \neq c_2)$, respectively. Take $\widetilde{U}_{\rm CPF}^{i,j}$ as an example, assume that the two logic-qubits are in superposition state, $a|\widetilde{0}\rangle_i|\widetilde{0}\rangle_j + b|\widetilde{0}\rangle_i|\widetilde{1}\rangle_j + c|\widetilde{1}\rangle_i|\widetilde{0}\rangle_j + d|\widetilde{1}\rangle_i|\widetilde{1}\rangle_j$, where a, b, c and d are normalized constants. The $\widetilde{U}_{{\rm CPF}|\widetilde{0}\rangle|\widetilde{0}\rangle}^{i,j}$ operation can be implemented according to following path. A single-photon pulse in state $(1/\sqrt{2})(|h\rangle + |v\rangle)$ is input from the port i, passes through PBS, and reaches the cavity i. The operations $\sigma_{x,i}^1 U_{\rm CPF} \sigma_{x,i}^1$ are needed to perform, i.e.,

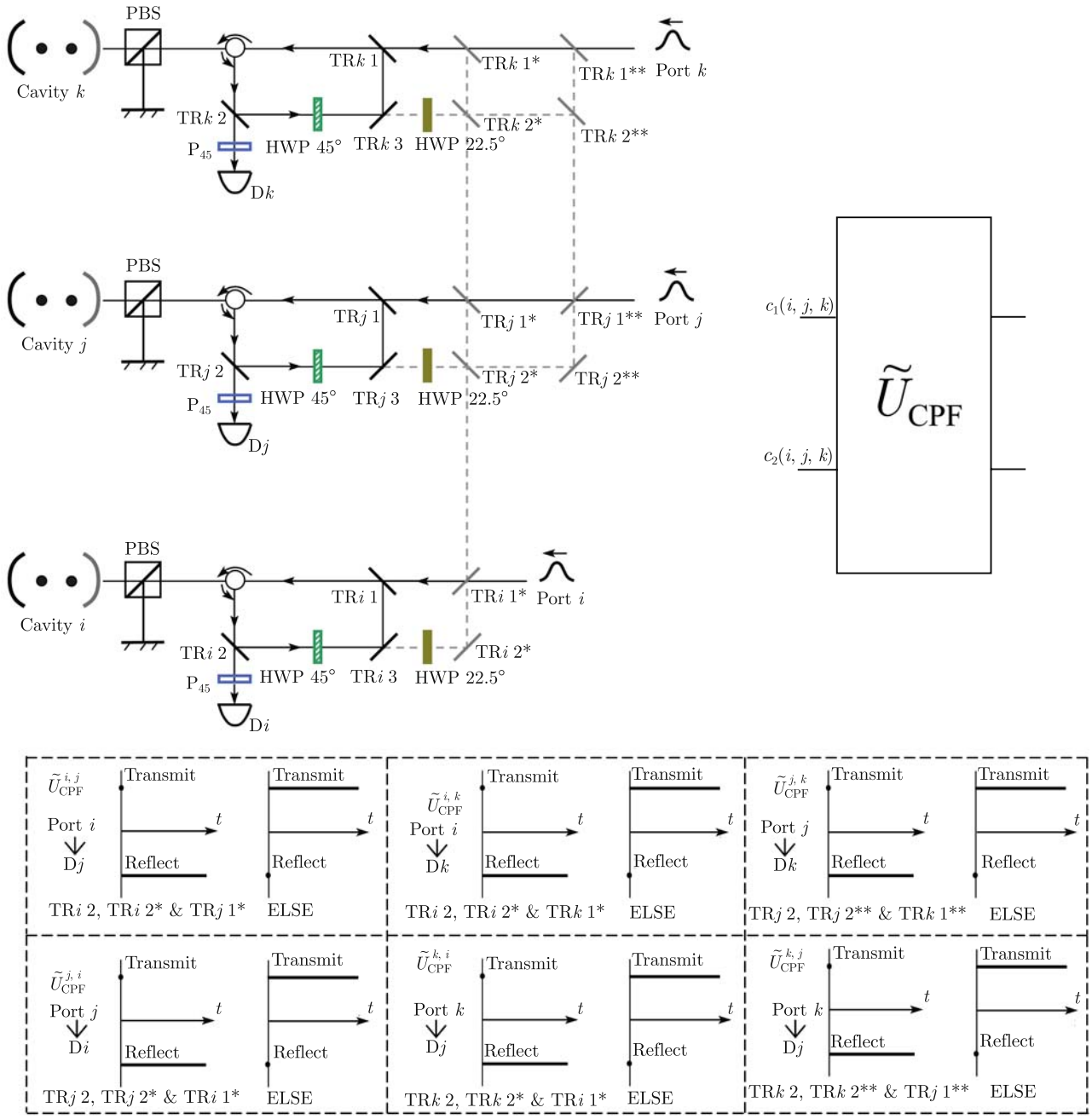

Fig. 8 Improved schematic setup for two logic-qubit controlled phase flip $\widetilde{U}^{c_1,c_2}_{\mathrm{CPF}}(c_1, c_2 = i, j, k, c_1 \neq c_2)$ which uses the additional channel shown by dashed gray lines and gray TRs. HWP 22.5° performs a Hadamard gate on the photon polarization states. The single-photon pulse's path for $\widetilde{U}^{i,j}_{\mathrm{CPF}}$ ($\widetilde{U}^{j,i}_{\mathrm{CPF}}$) is: port i -TRi 1*-TRi 1-C-PBS-Cavity i-PBS-C-TRi 2-HWP 45°-TRi 3-HWP 22.5°-TRi 2*-TRi 1* -TRj 2*-TRj 1*-TRj 1 -C-PBS-Cavity j-PBS-C-TRj 2-P_{45}-Dj (port j-TRj 1**-TRj 1*-TRj 1-C -PBS-Cavity j -PBS-C-TRj 2-HWP 45°-TRj 3–HWP 22.5°-TRj 2*-TRi 1*-TRi 1-C- PBS-Cavity i-PBS-C-TRi 2-P_{45}-Di). The control sequences for the other symmetric operations $\widetilde{U}^{c_1,c_2}_{\mathrm{CPF}}$ of TRs are listed. Compared to $\widetilde{H}$, the TRs keep unchanged during the controlled phase flip gating. For convenience of description below for Grover search, this operation is denoted by a block $\widetilde{U}_{\mathrm{CPF}}$.

σ_x operation on the atom 1 in cavity i before and after the single-photon pulse is reflected by the cavity i. Because of reflection of TRi 2, the single-photon pulse passes through HWP 45° and goes into the node j by the additional quantum channel. After going through HWP 22.5° and reflected by TRj 1*, the single-photon pulse arrives at the PBS and then the cavity j. As previously, we have to perform $\sigma^2_{x,j} U_{\mathrm{CPF}} \sigma^2_{x,j}$, i.e., the σ_x operation, on the atom 2 in the cavity j before and after the single-photon pulse is reflected by the cavity j. Then the

single-photon pulse goes through P_{45} and would be detected by Dj. The $\widetilde{U}^{i,j}_{\mathrm{CPF}|\widetilde{0}\rangle|\widetilde{0}\rangle}$ operation processed above can be shown step by step as:

$$\begin{aligned}
\widetilde{U}^{i,j}_{\mathrm{CPF}|\widetilde{0}\rangle|\widetilde{0}\rangle} &: \frac{1}{\sqrt{2}}(|h\rangle+|v\rangle)\otimes(a|\widetilde{0}\rangle_i|\widetilde{0}\rangle_j \\
&+b|\widetilde{0}\rangle_i|\widetilde{1}\rangle_j+c|\widetilde{1}\rangle_i|\widetilde{0}\rangle_j+d|\widetilde{1}\rangle_i|\widetilde{1}\rangle_j)\xrightarrow{\sigma^1_{x,i}U_{\mathrm{CPF}}\sigma^1_{x,i}} \\
&\frac{1}{\sqrt{2}}[a(|h\rangle+|v\rangle)|\widetilde{0}\rangle_i|\widetilde{0}\rangle_j+b(|h\rangle+|v\rangle)|\widetilde{0}\rangle_i|\widetilde{1}\rangle_j \\
&+c(-|h\rangle+|v\rangle)|\widetilde{1}\rangle_i|\widetilde{0}\rangle_j \\
&+d(-|h\rangle+|v\rangle)|\widetilde{1}\rangle_i|\widetilde{1}\rangle_j] \\
&\xrightarrow{\text{HWP }45^\circ,\text{ HWP }22.5^\circ} a|h\rangle|\widetilde{0}\rangle_i|\widetilde{0}\rangle_j+b|h\rangle|\widetilde{0}\rangle_i|\widetilde{1}\rangle_j \\
&+c|v\rangle|\widetilde{1}\rangle_i|\widetilde{0}\rangle_j+d|v\rangle|\widetilde{1}\rangle_i|\widetilde{1}\rangle_j \\
&\xrightarrow{\sigma^2_{x,j}U_{\mathrm{CPF}}\sigma^2_{x,j},P_{45}} \frac{1}{\sqrt{2}}(|h\rangle+|v\rangle)\otimes(-a|\widetilde{0}\rangle_i|\widetilde{0}\rangle_j \\
&+b|\widetilde{0}\rangle_i|\widetilde{1}\rangle_j+c|\widetilde{1}\rangle_i|\widetilde{0}\rangle_j+d|\widetilde{1}\rangle_i|\widetilde{1}\rangle_j)
\end{aligned} \tag{14}$$

To ensure the success of the operation $\widetilde{U}^{i,j}_{\mathrm{CPF}|\widetilde{0}\rangle|\widetilde{0}\rangle}$, a click of D$j$ is expected. The silence of Dj means failure and we must repeat the above steps from the very beginning. A similar process according to Eq. (14) can be done to the symmetric two-logic-qubits gate $\widetilde{U}^{j,i}_{\mathrm{CPF}|\widetilde{0}\rangle|\widetilde{0}\rangle}$, where the single-photon pulse is input from port j, as shown in Fig. 8. As we mentioned above, the single-logic-qubit Hadamard operation and the two-logic-qubit conditional operation are coexisting and could work independently by controlling TRs, the TRi 1*, TRi 2* (or TRj 1*, TRj 2*, TRj 1** and TRj 2** for node j), whose function is to connect spatially separated nodes, has no action during the single-logic-qubit Hadamard operation. Therefore, we can keep them always on in transmitting state during the time the $\widetilde{H}$ operation is carried out in individual nodes.

Different target items in Grover search need different controlled phase flip operation. Other phase flip gates in DFS, $\widetilde{U}_{\mathrm{CPF}|\widetilde{0}\rangle|\widetilde{1}\rangle}$, $\widetilde{U}_{\mathrm{CPF}|\widetilde{1}\rangle|\widetilde{0}\rangle}$, and $\widetilde{U}_{\mathrm{CPF}|\widetilde{1}\rangle|\widetilde{1}\rangle}$ can be implemented in a similar way without the need for assistant operations. This can reduce the experimental complexity. The operation process for different $\widetilde{U}_{\mathrm{CPF}}$ depends on the single physical qubit σ_x operation on a different atom in the cavity. The corresponding operation processes can be shown step by step as:

$$\begin{aligned}
\widetilde{U}^{i,j}_{\mathrm{CPF}|\widetilde{0}\rangle|\widetilde{1}\rangle} &: \frac{1}{\sqrt{2}}(|h\rangle+|v\rangle)\otimes(a|\widetilde{0}\rangle_i|\widetilde{0}\rangle_j \\
&+b|\widetilde{0}\rangle_i|\widetilde{1}\rangle_j+c|\widetilde{1}\rangle_i|\widetilde{0}\rangle_j+d|\widetilde{1}\rangle_i|\widetilde{1}\rangle_j) \\
&\xrightarrow{\sigma^1_{x,i}U_{\mathrm{CPF}}\sigma^1_{x,i}} \frac{1}{\sqrt{2}}[a(|h\rangle+|v\rangle)|\widetilde{0}\rangle_i|\widetilde{0}\rangle_j+b(|h\rangle+|v\rangle)|\widetilde{0}\rangle_i|\widetilde{1}\rangle_j \\
&+c(-|h\rangle+|v\rangle)|\widetilde{1}\rangle_i|\widetilde{0}\rangle_j+d(-|h\rangle+|v\rangle)|\widetilde{1}\rangle_i|\widetilde{1}\rangle_j] \\
&\xrightarrow{\text{HWP }45^\circ,\text{HWP }22.5^\circ} a|h\rangle|\widetilde{0}\rangle_i|\widetilde{0}\rangle_j+b|h\rangle|\widetilde{0}\rangle_i|\widetilde{1}\rangle_j \\
&+c|v\rangle|\widetilde{1}\rangle_i|\widetilde{0}\rangle_j+d|v\rangle|\widetilde{1}\rangle_i|\widetilde{1}\rangle_j \\
&\xrightarrow{\sigma^1_{x,j}U_{\mathrm{CPF}}\sigma^1_{x,j},P_{45}} \frac{1}{\sqrt{2}}(|h\rangle+|v\rangle)\otimes(a|\widetilde{0}\rangle_i|\widetilde{0}\rangle_j \\
&-b|\widetilde{0}\rangle_i|\widetilde{1}\rangle_j+c|\widetilde{1}\rangle_i|\widetilde{0}\rangle_j+d|\widetilde{1}\rangle_i|\widetilde{1}\rangle_j)
\end{aligned} \tag{15}$$

$$\begin{aligned}
\widetilde{U}^{i,j}_{\mathrm{CPF}|\widetilde{1}\rangle|\widetilde{0}\rangle} &: \frac{1}{\sqrt{2}}(|h\rangle+|v\rangle)\otimes(a|\widetilde{0}\rangle_i|\widetilde{0}\rangle_j+b|\widetilde{0}\rangle_i|\widetilde{1}\rangle_j \\
&+c|\widetilde{1}\rangle_i|\widetilde{0}\rangle_j+d|\widetilde{1}\rangle_i|\widetilde{1}\rangle_j) \\
&\xrightarrow{\sigma^2_{x,i}U_{\mathrm{CPF}}\sigma^2_{x,i}} \frac{1}{\sqrt{2}}[a(-|h\rangle+|v\rangle)|\widetilde{0}\rangle_i|\widetilde{0}\rangle_j \\
&+b(-|h\rangle+|v\rangle)|\widetilde{0}\rangle_i|\widetilde{1}\rangle_j \\
&+c(|h\rangle+|v\rangle)|\widetilde{1}\rangle_i|\widetilde{0}\rangle_j+d(|h\rangle+|v\rangle)|\widetilde{1}\rangle_i|\widetilde{1}\rangle_j] \\
&\xrightarrow{\text{HWP }45^\circ,\text{ HWP }22.5^\circ} a|v\rangle|\widetilde{0}\rangle_i|\widetilde{0}\rangle_j+b|v\rangle|\widetilde{0}\rangle_i|\widetilde{1}\rangle_j \\
&+c|h\rangle|\widetilde{1}\rangle_i|\widetilde{0}\rangle_j+d|h\rangle|\widetilde{1}\rangle_i|\widetilde{1}\rangle_j \\
&\xrightarrow{\sigma^2_{x,j}U_{\mathrm{CPF}}\sigma^2_{x,j},P_{45}} \frac{1}{\sqrt{2}}(|h\rangle+|v\rangle)\otimes(a|\widetilde{0}\rangle_i|\widetilde{0}\rangle_j \\
&+b|\widetilde{0}\rangle_i|\widetilde{1}\rangle_j-c|\widetilde{1}\rangle_i|\widetilde{0}\rangle_j+d|\widetilde{1}\rangle_i|\widetilde{1}\rangle_j)
\end{aligned} \tag{16}$$

$$\begin{aligned}
\widetilde{U}^{i,j}_{\mathrm{CPF}|\widetilde{1}\rangle|\widetilde{1}\rangle} &: \frac{1}{\sqrt{2}}(|h\rangle+|v\rangle)\otimes(a|\widetilde{0}\rangle_i|\widetilde{0}\rangle_j \\
&+b|\widetilde{0}\rangle_i|\widetilde{1}\rangle_j+c|\widetilde{1}\rangle_i|\widetilde{0}\rangle_j+d|\widetilde{1}\rangle_i|\widetilde{1}\rangle_j) \\
&\xrightarrow{\sigma^2_{x,i}U_{\mathrm{CPF}}\sigma^2_{x,i}} \frac{1}{\sqrt{2}}[a(-|h\rangle+|v\rangle)|\widetilde{0}\rangle_i|\widetilde{0}\rangle_j \\
&+b(-|h\rangle+|v\rangle)|\widetilde{0}\rangle_i|\widetilde{1}\rangle_j \\
&+c(|h\rangle+|v\rangle)|\widetilde{1}\rangle_i|\widetilde{0}\rangle_j+d(|h\rangle+|v\rangle)|\widetilde{1}\rangle_i|\widetilde{1}\rangle_j] \\
&\xrightarrow{\text{HWP }45^\circ,\text{ HWP }22.5^\circ} a|v\rangle|\widetilde{0}\rangle_i|\widetilde{0}\rangle_j+b|v\rangle|\widetilde{0}\rangle_i|\widetilde{1}\rangle_j \\
&+c|h\rangle|\widetilde{1}\rangle_i|\widetilde{0}\rangle_j+d|h\rangle|\widetilde{1}\rangle_i|\widetilde{1}\rangle_j \\
&\xrightarrow{\sigma^1_{x,j}U_{\mathrm{CPF}}\sigma^1_{x,j},P_{45}} \frac{1}{\sqrt{2}}(|h\rangle+|v\rangle)\otimes(a|\widetilde{0}\rangle_i|\widetilde{0}\rangle_j \\
&+b|\widetilde{0}\rangle_i|\widetilde{1}\rangle_j+c|\widetilde{1}\rangle_i|\widetilde{0}\rangle_j-d|\widetilde{1}\rangle_i|\widetilde{1}\rangle_j)
\end{aligned} \tag{17}$$

Although we only take $\widetilde{U}^{i,j}_{\mathrm{CPF}}$ as an example, the operations for $\widetilde{U}^{i,k}_{\mathrm{CPF}}$ and $\widetilde{U}^{j,k}_{\mathrm{CPF}}$ ($\widetilde{U}^{j,i}_{\mathrm{CPF}}$, $\widetilde{U}^{k,i}_{\mathrm{CPF}}$ and $\widetilde{U}^{k,j}_{\mathrm{CPF}}$) are similar. Moreover, for the cavity quantum network, we give the basic three cavities case in Fig. 8, the improved experiment setup compared to the previous one which is

only suitable to the two-qubit case [29] can easily extend to the N-qubit quantum network.

We have introduced the necessary logic-qubit operation gates in DFS, then we give the implementation for two-qubit Grover search in DFS in Fig. 9. Generally speaking, under the same physical system, it is very hard that two-qubit conditional phase operation and diffusion transform operation are both realized directly. As in Refs. [41, 42], the diffusion transform operation can be achieved directly by adding a strong resonant classical field, but the two-qubit controlled phase flip operation must utilize the combination of the Hadamard operation and the diffusion transform operation. In our scheme, for the diffusion transform operation, we use the operation combination $\widetilde{D} = \widetilde{H}^{\otimes 2}\widetilde{U}_{\rm CPF}\widetilde{H}^{\otimes 2}$, which the two-logic-qubit controlled phase flip operation can be done directly. It must be mentioned that, Fig. 9 is the sketched operation sequences for a special target item from left to right. Take $|\widetilde{0}\rangle|\widetilde{1}\rangle$ for example, the concrete operation for two-logic-qubit controlled phase flip operation is $\widetilde{U}^{c_1,c_2}_{{\rm CP}|\widetilde{0}\rangle|\widetilde{1}\rangle}$, and the c_1, c_2 stand for the photon pulse input port $(c_1, c_2 = i, j, k, c_1 \neq c_2)$.

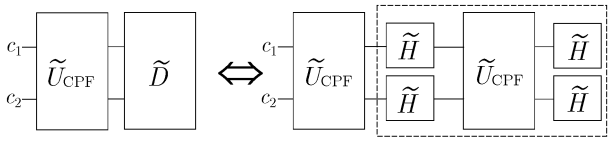

Fig. 9 Sketched operation sequences for Grover search in DFS, where the blocks $\widetilde{H}$ and $\widetilde{U}_{\rm CPF}$ are from Figs. 7 and 8. $\widetilde{D}$ uses the operation combination $\widetilde{H}^{\otimes 2}\widetilde{U}_{\rm CPF}\widetilde{H}^{\otimes 2}$. The sequential execution of operations is from left to right.

Different from the standard Grover search where the measurement is at the end of whole search process, each operation in the blocks in Fig. 9 has detection result at the ending. As shown in Figs. 7 and 8, each logic-qubit (or, say, node in DFS) has individual input port for photon pulses to complete the necessary operations, and different operational results can be distinguished by detecting output photons. That is, different operational results in each step are distinguishable in our scheme, (for example, the single-logic-qubit operation $\widetilde{H}_i$ in the ith cavity is associated with a single-photon pulse input in port i and the detector Di, whereas the two-logic-qubit operation $\widetilde{U}^{i,j}_{\rm CPF}$ is relevant to the input port i and the response of Dj), the successful detections of the single-photon pulses ensure the high fidelities of the gate operations.

Any multiparticle unitary operation can be decomposed into two kinds of elementary gates, i.e., one-qubit rotations and two-qubit conditional gates; our Grover search scheme in DFS can be extended in principle to the multi-logic-qubit case. However, the needed decomposition of the N-qubit gates will become more and more complicated with the increase of qubit number N, if the implementation of multiqubit condition gate cannot be completed directly. How to implement the multiqubit case in the cavity QED system is the urgent consideration for large scale QIP. Very recently, a nonlocal N-qubit conditional phase gate based on the same cavity-assisted interaction by single-photon pulses has been proposed [44] in this paper. We hope a compatible design which also works in DFS will be proposed in the near future.

The success of logic-qubit operations in DFS requires the switching time sequences of TRs to be implemented accurately [29]. During the operation $\widetilde{H}_i$ in Fig. 7, TRi 1 and TRi 2 will change their transmitting or reflecting state as needed. TRi 1 need to stay in transmitting state before the time $T_0 + T_1$, then it turns into a reflecting state. TRi 2 will turn the reflecting state into transmitting state at the time $2T_0 + T_1$, where T_0 is the time for single-photon pulse process TRi 1-C-PBS-Cavity-PBS-C-TRi 2, while T_1 is the time for TRi 2-HWP 45°-TRi 3-TRi 1. Actually, in addition to the time control sequences of TRi 1 and TRi 2 designed in Fig. 7, we have an alternative. Take TRi 1 for instance: Once the single-photon pulse from port i has gone through TRi 1, we change the transmitting state of the TRi 1 into reflecting state without waiting for the time T_0+T_1. While the TRs in the operation $\widetilde{U}_{\rm CPF}$, they keep unchanged during the conditional phase gating; for example, only TRi 2, TRi 2* and TRj 1* keeping in reflecting state and the other TRs keeping in transmitting state are needed in operation $\widetilde{U}^{i,j}_{\rm CPF}$.

It is promising to search for physical arrangements that are capable of carrying out a variety of QIP tasks without a significant modification of the setup itself. For example, for the cavity QED system, we hope it can do as much quantum information work as possible, such as preparation of entangled states, quantum state transfer, quantum search algorithms, and even quantum computation, under the similar setup condition. Compatible QIP is one direction in which researchers should develop, under the quantum state stability analysis against decoherence and the single-photon interaction to induce the efficient multiparty entanglement. In our scheme for qubits encoded in pairs of atoms in DFS, we can implement transfer and teleportation of quantum states [29] and preparation of entangled states [28]. Compared with the previous four remote atomic qubits entangled states preparation, we can expand entanglement of GHZ states and cluster states to arbitrary N-qubit situation instead of only the even number qubit case. For ex-

ample, three-logic-qubit GHZ state can be completed by $|\widetilde{0}\rangle_1|\widetilde{0}\rangle_2|\widetilde{0}\rangle_3 \xrightarrow{\widetilde{H}_1} \frac{1}{\sqrt{2}}(|\widetilde{0}\rangle+|\widetilde{1}\rangle)_1|\widetilde{0}\rangle_2|\widetilde{0}\rangle_3 \xrightarrow{\widetilde{C}^{1,2}_{\rm NOT}} \frac{1}{\sqrt{2}}(|\widetilde{00}\rangle+|\widetilde{11}\rangle)_{12}|\widetilde{0}\rangle_3 \xrightarrow{\widetilde{C}^{2,3}_{\rm NOT}} \frac{1}{\sqrt{2}}(|\widetilde{0}\rangle_1|\widetilde{0}\rangle_2|\widetilde{0}\rangle_3 + |\widetilde{1}\rangle_1|\widetilde{1}\rangle_2|\widetilde{1}\rangle_3)$, where $\widetilde{C}^{i,j}_{\rm NOT} = \widetilde{H}_j \otimes \widetilde{U}^{i,j}_{\rm CP} \otimes \widetilde{H}_j$. Although we also gave a the discussion of cluster state in Section 2, we did not give the crucial single-logic-qubit Hadamard operation. With the help of $\widetilde{H}$, the standard operations for three-qubit cluster state is, $|\widetilde{0}\rangle_1|\widetilde{0}\rangle_2|\widetilde{0}\rangle_3 \xrightarrow{\widetilde{H}_1,\widetilde{H}_2,\widetilde{H}_3} \frac{1}{2^{3/2}}(|\widetilde{0}\rangle + |\widetilde{1}\rangle)_1(|\widetilde{0}\rangle + |\widetilde{1}\rangle)_2(|\widetilde{0}\rangle+|\widetilde{1}\rangle)_3 \xrightarrow{\widetilde{U}^{1,2}_{{\rm CPF}|\widetilde{1}\rangle|\widetilde{1}\rangle},\widetilde{U}^{2,3}_{{\rm CPF}|\widetilde{1}\rangle|\widetilde{1}\rangle}} \frac{1}{2^{3/2}}(|\widetilde{0}\rangle+|\widetilde{1}\rangle\widetilde{\sigma}^2_z)_1(|\widetilde{0}\rangle+|\widetilde{1}\rangle\widetilde{\sigma}^3_z)_2(|\widetilde{0}\rangle + |\widetilde{1}\rangle)_3$.

The tailored experimental setup improve the scalability of the quantum network of cavity QED system. Large-scale QIP allow efficient connection of arbitrary two nodes instead of the nearest neighbor case [29]. Without loss of generality, the setup in Fig. 8 gives a three-qubit example including the operation's symmetry. The obstacles of scalability of our scheme, except the intrinsic defect of the apparatus, are the growing complexity of the additional channels which is used to connect different nodes followed with the large logic-qubit number. We hope a more advanced high performance integrated device can be competent for the public channels in the near future.

5 Construct multiqubit network in DFS

In quantum information science, one-qubit rotations and two-qubit conditional operations could constitute universal quantum computing (QC) [45]. Although these basic operations have been achieved experimentally in various systems, to have a large-scale QC efficiently with high-fidelity, we are still exploring for a direct accomplishment of many-qubit conditional gates to simplify the operational steps and decrease the implementing time.

With the error protection encoding using DFS, we will propose a nonlocal many-qubit gating in DFS in a quantum network constituted by cavities, based on cavity-assisted interaction by single-photon interference [46]. To make our description clear, we will take the three-logic-qubit Toffoli gate as an example, and our idea is directly applicable to the case of arbitrary numbers of logic qubits. The favorable features of our scheme include a big reduction of the implementational steps compared to conventional methods by the network of one- and two-qubit quantum gates. Besides, the Hadamard operation of the single-logic-qubit and multi-logic-qubit conditional operations could coexist in our design but work independently due to our elaborate control of the path of the single-photons, which helps for compatibility of the quantum network. Furthermore, our network allows quantum communications between arbitrary two cavity nodes.

With the cavity-assisted photon scattering, both the single-logic-qubit Hadamard gate $\widetilde{H}$ and the two-logic-qubit conditional phase gate $\widetilde{U}_{\rm CP2}$ had been realized between two neighboring nodes in a cavity-based system [29], where $\widetilde{H}$ depends on twice interactions of the photon with the cavity and $\widetilde{U}_{\rm CP2}$ needs only one interaction with each cavity. To extend our idea to be more than two cavities, we need to design a more smart device. Figure 10 demonstrates from different views the basic unit of such a design, where the half-wave plate 45° (HWP 45°), with its axis at 45° to the horizontal direction, rotates the photon polarization as $|h\rangle \leftrightarrow |v\rangle$. HWP 22.5°, at an angle of 22.5° to the horizontal direction, performs a Hadamard gate on the photon polarization states, i.e., $|h\rangle \leftrightarrow (|h\rangle+|v\rangle)/\sqrt{2}$, $|v\rangle \leftrightarrow (|h\rangle-|v\rangle)/\sqrt{2}$. C and C* are circulators. P_{45} is a 45° polarizer projecting the polarization $(|h\rangle+|v\rangle)/\sqrt{2}$. The different graphic denotations of PBS and TR are due to different views.

TR, marked in purple, including TR0, TR1, TR2, TR3, TRin and TRout in Fig. 10, are optical devices which can be controlled exactly as needed to transmit or reflect a photon with a very fast switching time. All the TR devices are identical, but labeled to be TRm ($m = 0, 1, 2, \cdots$) for convenience of our description. STR, a special device that controls the path of the photon to different planes, has three ports allowing the single-photon pulses to communicate with the cavity node. The lines in different colors in Fig. 10 show the different photon paths of the three ports, respectively. The single-photon pulse can enter the cavity node directly from the port 0 along the black line depending on the transmitting states of TRin and TRout, as shown in the top plot of Fig. 10(b). Alternatively, STR allows the photon input from port 1 following the light red line [Fig. 10(c2)]. After its interaction with the atoms in the cavity, the single-photon pulse should move along the light blue line going to TR2 and then be reflected out of the node from port 2 [Fig. 10(c1)]. Moreover, if it just passes by the cavity node, the single-photon pulse will pass through STR from the port 1 directly to port 2 with the help of TR1 and TR3, as shown in Fig. 10(c3).

Within the cavity node, the movement of the single-photon pulse also depends on the state of TR0. When TR0 is switched to a transmitting state, the photon will pass through TR0 and P_{45} and then be measured by the detector directly. This is part of the way for $\widetilde{H}$ [29]. To carry out conditional gates, we require TR0 to stay

in a reflecting state, which makes the photon go out of the cavity node along the light blue line from the port 2. To implement our scheme, we have to switch the relevant TR into the corresponding transmitting or reflecting state according the photon paths in Fig. 10.

Based on the above basic unit, we construct a circular many-qubit cavity network in DFS in Fig. 11. To make our description clear and simple, without loss of gen-

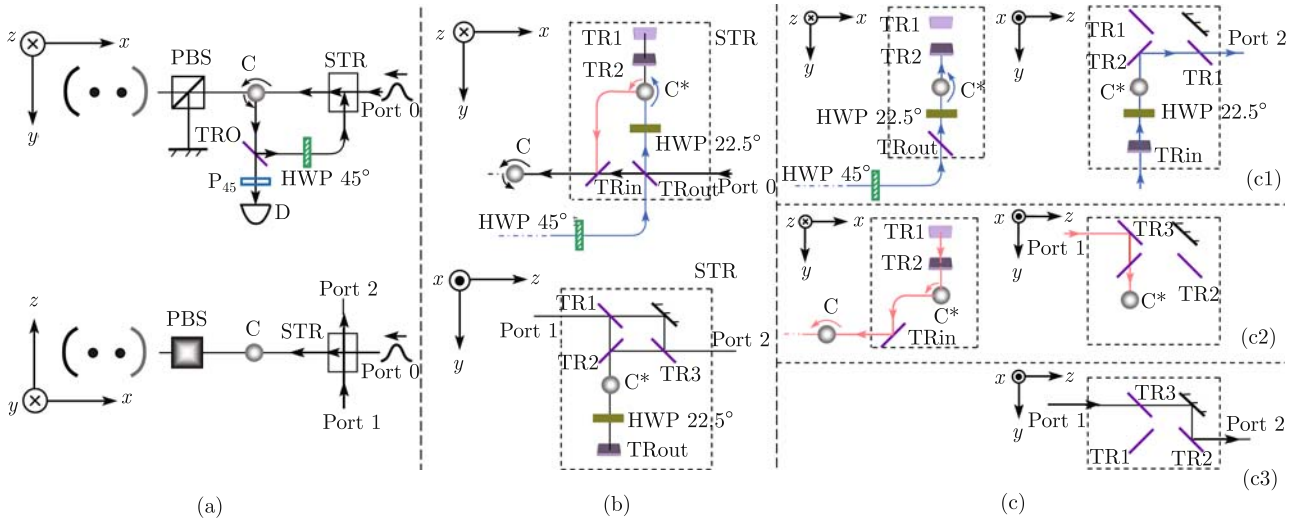

Fig. 10 Schematic setup of the basic node unit of our design from different views. **(a)** Setup viewed along z-axis and viewed on the x-z plane; **(b)** The configuration of STR, which consists of several optical elements, such as TR (marking in purple) , circulator and haft-wave plate. STR can control the path of the photon to different planes (see text for detail). The single-photon pulse can enter the cavity node directly from the port 0 (along the black line); **(c)** The photon can be guided in the cavity node from the port 1 (along the light red line), and be guided out of the cavity node from the port 2 (along the light blue line). Furthermore, the photon can cross STR directly between port 1 and port 2. HWP 45° rotates the photon polarization as $|h\rangle \leftrightarrow |v\rangle$, HWP 22.5° perform Hadamard operation on the photon state. D is a detector, C and C* are circulators, P_{45} is a 45° polarizer. TR can be controlled exactly as needed to transmit or to reflect a photon.

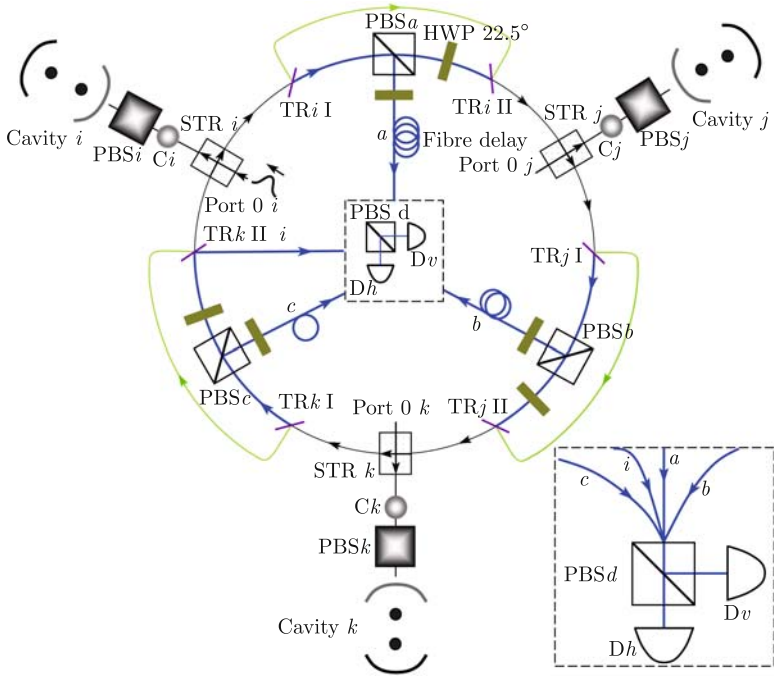

Fig. 11 Schematic setup for implementation of three-logic-qubit conditional phase gate $\widetilde{U}_{\rm CP3}$ by single-photon interference in clock-wise direction. The photon will take four possible paths a, b, c and i to reach PBSd. The single-logic-qubit Hadamard operation and the two- and multi-logic-qubit conditional operation are coexisting in our scheme but could work independently by controlling the path of the single-photons. The dark blue circle is the necessary path for the $\widetilde{U}_{\rm CP3}$ operation, and the green path for the $\widetilde{U}_{\rm CP2}$ between two logic qubits. Each dark-green half-wave plate stands for a HWP 22.5°. The inset is for the detection made at the center of the network.

erality, we only demonstrate a three-logic-qubit Toffoli gate $\widetilde{T}^{ij,k}_{\rm offoli} = \widetilde{H}_k \otimes \widetilde{U}_{\rm CP3} \otimes \widetilde{H}_k$ as an example, where $\widetilde{H}_k$ and $\widetilde{U}_{\rm CP3}$ are Hadamard gate on the kth logic-qubit and three-logic-qubit conditional phase gate, respectively. For the many-qubit conditional gate, the key point is not the order of the operations on individual nodes, but the phase flip when all target logic-qubits are in states $|\widetilde{1}\rangle$. So as an example, we give in Fig. 11 an implementation of $\widetilde{U}_{\rm CP3}$ by a clock-wise operation based on the single-photon interference.

The operation of $\widetilde{U}_{\rm CP3}$ as shown in Fig. 11 will follow the dark blue optical path on the circle. It can be performed by the following steps. A single-photon pulse in state $(|h\rangle + |v\rangle)/\sqrt{2}$ is imported from the port $0i$, i.e., the port 0 belonging to the ith node. As mentioned previously in Fig. 10, the input photon will enter the node i directly through STRi, and reach the cavity i through C and PBS. To have the operation $U_{\rm CPF}$, we perform a σ_x operation on the atom 2 in the cavity i (denoted as $\sigma^2_{x,i}$) so that $U_{\rm CPF}$ could happen when the single-photon pulse moves in and then out of the cavity. Then we carry out another σ_x operation to restore the state of the atom 2. Subsequently, the photon moves back to C again, turned by C and then reflected by TR0 to HWP 45°. Finally, the single-photon pulse moves out of the node i from the port $2i$ of STRi. Let us turn to Fig. 11 again. After the single-photon pulse moves out of the node i, it clockwisely arrives at PBSa through TRi I along the dark blue line. Whether the photon pulse will pass through PBSa to node j or be reflected along the path$a$ to PBSd depends on the state of the logic-qubit inside the node i (i.e., cavity i). Specifically, for the logic-qubit in cavity i in state $|\widetilde{0}\rangle_i$ or $|\widetilde{1}\rangle_i$, the above photon path in the basic unit leads to

$$\begin{aligned}
&\frac{|h\rangle + |v\rangle}{\sqrt{2}}|\widetilde{0}\rangle_i \xrightarrow{\sigma^2_{x,i}U_{\rm CPF}\sigma^2_{x,i}} \frac{-|h\rangle + |v\rangle}{\sqrt{2}}|\widetilde{0}\rangle_i \\
&\xrightarrow{\text{HWP } 45^\circ} \frac{|h\rangle - |v\rangle}{\sqrt{2}}|\widetilde{0}\rangle_i \\
&\xrightarrow{\text{HWP } 22.5^\circ} |v\rangle|\widetilde{0}\rangle_i \frac{|h\rangle + |v\rangle}{\sqrt{2}}|\widetilde{1}\rangle_i
\end{aligned} \tag{18}$$

$$\begin{aligned}
&\xrightarrow{\sigma^2_{x,i}U_{\rm CFP}\sigma^2_{x,i}} \frac{|h\rangle + |v\rangle}{\sqrt{2}}|\widetilde{1}\rangle_i \\
&\xrightarrow{\text{HWP } 45^\circ} \frac{|h\rangle + |v\rangle}{\sqrt{2}}|\widetilde{1}\rangle_i \\
&\xrightarrow{\text{HWP } 22.5^\circ} |h\rangle|\widetilde{1}\rangle_i
\end{aligned} \tag{19}$$

Therefore, if the logic-qubit in the cavity is in state $|\widetilde{0}\rangle$, the single-photon pulse will be reflected by PBSa to go along the path$a$, whereas the photon will go through PBSa and HWP 22.5° to the node j if the atoms are in $|\widetilde{1}\rangle$. For the latter case, the h-polarized photon will go through a HWP 22.5° before entering the cavity node j, and thereby becomes in superposition $(|h\rangle + |v\rangle)1/\sqrt{2}$ again. The interaction between the photon pulse and the atoms in cavity j is similar to the cavity i, and the subsequent process to the cavity$k$ is similar to that the cavity j. In our three-logic-qubit case, the whole optical path ends at reaching the detector Dh or Dv along the path i. The click of Dv yields a minus sign in front of the state $|\widetilde{1}\rangle_i|\widetilde{1}\rangle_j|\widetilde{1}\rangle_k$, and the click of D$h$ means nothing changed. Straightforward deduction could show that, for three logic-qubits initially in an arbitrary state $\beta_1|\widetilde{0}\rangle_i|\widetilde{0}\rangle_j|\widetilde{0}\rangle_k + \beta_2|\widetilde{0}\rangle_i|\widetilde{0}\rangle_j|\widetilde{1}\rangle_k + \beta_3|\widetilde{0}\rangle_i|\widetilde{1}\rangle_j|\widetilde{0}\rangle_k + \beta_4|\widetilde{0}\rangle_i|\widetilde{1}\rangle_j|\widetilde{1}\rangle_k + \beta_5|\widetilde{1}\rangle_i|\widetilde{0}\rangle_j|\widetilde{0}\rangle_k + \beta_6|\widetilde{1}\rangle_i|\widetilde{0}\rangle_j|\widetilde{1}\rangle_k + \beta_7|\widetilde{1}\rangle_i|\widetilde{1}\rangle_j|\widetilde{0}\rangle_k + \beta_8|\widetilde{1}\rangle_i|\widetilde{1}\rangle_j|\widetilde{1}\rangle_k$, the above process yields

$$\begin{aligned}
&\frac{|h\rangle}{\sqrt{2}} \otimes (\beta_1|\widetilde{0}\rangle_i|\widetilde{0}\rangle_j|\widetilde{0}\rangle_k + \beta_2|\widetilde{0}\rangle_i|\widetilde{0}\rangle_j|\widetilde{1}\rangle_k + \beta_3|\widetilde{0}\rangle_i|\widetilde{1}\rangle_j|\widetilde{0}\rangle_k \\
&+\beta_4|\widetilde{0}\rangle_i|\widetilde{1}\rangle_j|\widetilde{1}\rangle_k + \beta_5|\widetilde{1}\rangle_i|\widetilde{0}\rangle_j|\widetilde{0}\rangle_k + \beta_6|\widetilde{1}\rangle_i|\widetilde{0}\rangle_j|\widetilde{1}\rangle_k \\
&+\beta_7|\widetilde{1}\rangle_i|\widetilde{1}\rangle_j|\widetilde{0}\rangle_k + \beta_8|\widetilde{1}\rangle_i|\widetilde{1}\rangle_j|\widetilde{1}\rangle_k) - \frac{|v\rangle}{\sqrt{2}} \otimes (\beta_1|\widetilde{0}\rangle_i|\widetilde{0}\rangle_j|\widetilde{0}\rangle_k \\
&+\beta_2|\widetilde{0}\rangle_i|\widetilde{0}\rangle_j|\widetilde{1}\rangle_k + \beta_3|\widetilde{0}\rangle_i|\widetilde{1}\rangle_j|\widetilde{0}\rangle_k + \beta_4|\widetilde{0}\rangle_i|\widetilde{1}\rangle_j|\widetilde{1}\rangle_k \\
&+\beta_5|\widetilde{1}\rangle_i|\widetilde{0}\rangle_j|\widetilde{0}\rangle_k + \beta_6|\widetilde{1}\rangle_i|\widetilde{0}\rangle_j|\widetilde{1}\rangle_k + \beta_7|\widetilde{1}\rangle_i|\widetilde{1}\rangle_j|\widetilde{0}\rangle_k \\
&-\beta_8|\widetilde{1}\rangle_i|\widetilde{1}\rangle_j|\widetilde{1}\rangle_k)
\end{aligned} \tag{20}$$

The measurement is made on the output photon by detectors Dh and Dv behind PBSd. As PBS transmits (reflects) h (v)-polarized photon, according to Eq. (19), the three-logic-qubit conditional phase gate $\widetilde{U}_{\rm CP3}$ succeeds if Dv clicks. With the help of single-logic-qubit $\widetilde{H}$ operation, we can carry out a standard Toffoli gate in DFS by $\widetilde{T}^{ijk}_{\rm offoli} = \widetilde{H}_k \otimes \widetilde{U}_{\rm CP3} \otimes \widetilde{H}_k$. It must be mentioned that the optical length of the paths a, b, c and i must be equal to suppress the phase instability in the single-photon interference.

Different operations can be distinguished from the corresponding ports and detectors. The single-logic-qubit operation $\widetilde{H}_i$ in the ith cavity is associated with a single-photon pulse input from the port $0i$ and output to the detector Di [29], whereas the many-qubit gating is related to the input from the port $0i$ and the output to the detector Dv. Since different gates could coexist in our design and work independently, our design is not only scalable but also compact.

It is evident that our scheme can be directly extended to be more than the three-node case. Meanwhile, it could implement the conditional phase flip between two arbitrary nodes. For example, by switching TRi (including TRi I and TRi II) to the reflecting state, we may have the single-photon pulse skipping over PBSa. When it arrives at the STRj, the single-photon pulse can also

be chosen entering node$j$ or not according to Fig. 10(c). In this case, we can implement the communications between two arbitrary nodes instead of only the neighboring nodes [29].

The currently achieved technology of deterministic single-photon source [47], with 10 000 high-quality single photons generated continuously per second, supports a fast implementation of our scheme. About the logic-qubits, we may confine the atoms in optical lattices embedded in an optical cavity which has already been achieved experimentally [48]. However, current techniques have not yet enabled the atoms individually confined in some particular lattice sites. Alternatively, we may consider two charged atoms confined by a trap potential and optically coupled by the cavity mode. A single Calcium ion has been successfully trapped in such a device [50]. To achieve our scheme, however, we require the above experiment to be extended to two ions.

For the cavity-assisted operation $U_{\rm CPF}$, the numerical simulations had been made in Ref. [25−27], which shows that, if the duration T for the photon pulse input in the cavity and the cavity decay rate κ satisfy $\kappa T \gg 1$, $U_{\rm CPF}$ is insensitive to both the atom-cavity coupling strength and the Lamb-Dicke localization. Specifically, if $\kappa T \sim 100$ and the atom-cavity coupling is several times stronger than the dissipative rates of the system, the gate fidelity is almost unity ($F > 99.5\%$)[25−27]. Therefore, with the experimental numbers $\kappa/(2\pi) \sim 4$ MHz, $g/(2\pi) \sim 30$ MHz, $\Gamma/(2\pi) \sim 2.6$ MHz [50−52], we may estimate the time for $U_{\rm CPF}$ and $\widetilde{H}$ to be about $3 \sim 5$ μs and $6 \sim 10$ μs, respectively, for $\kappa T \gg 1$. The time of the $\widetilde{U}_{{\rm CP}N}$ operation depends on the number of the logic qubits. For example, for the case of N =3, 4 and 5, the gating time of $\widetilde{U}_{{\rm CP}N}$ would be about ~ 12 μs, ~ 16 μs and ~ 20 μs, respectively.

The possible imperfection is mainly from the photon loss, the phase instability, detector inefficiency, and other logic errors beyond collective dephasing in real QC operations, such as leakage errors and so on. Like the repeat-until-success scheme [53] which discards the photon loss events by photon detection, our scheme could reach high fidelity by the photon detection even in the case of photon loss. Besides, the phase stability could be guaranteed by keeping the path lengths of the photons stable at sub-wavelength levels. Moreover, the current dark count rate of the single-photon detector is about 100 Hz, which could reduce the efficiency of our scheme by a factor of 10^{-4}. However, this is not an intrinsic drawback of our scheme itself. As for the logic errors beyond collective dephasing, we may suppress them by some elaborately designed pulse sequences, e.g., with "Bang-Bang" control pulses on the encoded qubits and then amended by refocusing on individual physical qubits [54], or with some specially designed pulses [55]. To suppress these unpredictable errors, we have to mention two points below. First, we have supposed in our model that the collective dephasing errors are dominant for the atomic qubits in a cavity at very low temperature, which implies that the quantum gating with DFS employed in our scheme should behave better than others without using DFS. The second point is that both "Bang-Bang" control and refocusing have sophisticated techniques. Therefore, all the errors would be strongly suppressed.

6 Summary

In summary, we have focused on the operations of the logic qubits including the preparation of entangled states, information transfer and teleportation of quantum states, two-qubit Grover search and how to construct the quantum network in DFS, within the cavity QED regime based on a cavity-assisted interaction by single-photon pulses. We hope that our work could be helpful for developing distributed quantum information processing.

Acknowledgements We acknowledge Prof. Mang Feng for fruitful discussions. This work was partly supported by the National Natural Science Foundation of China under Grant Nos. 10774163 and 60490280, and partly by NFRP under grant No. 2006CB921203.

References

1. D. Deutsch, Quantum theory, the Church-Turing Principle and the universal quantum computer, Proc. R. Soc. Lond. A, 1985, 400: 97
2. P. W. Shor, Algorithms for quantum computation: discrete logarithms and factoring, In: Proceeding of the 35th Annual Symposium on Foundations of Computer Science, Los Alamitos: IEEE Computer Society Press, 1994: 124
3. L. K. Grover, A Fast Quantum Mechanics Algorithm for Database Search, Proceedings, 28th ACM Symposium on Theory of Computation, New York: ACM Press, 1996: 212
4. D. P. DiVincenzo, Fortschr. Phys., 2000, 48: 771
5. J. I. Cirac and P. Zoller, Phys. Rev. Lett., 1995, 74: 4091
6. M. Šašura and V. Bužek, J. Mod. Opt., 2002, 49: 1593
7. J.-Y. Wan, Y.-Z. Wang, and L. Liu, Front. Phys. China, 2007, 2: 375
8. P. Kok, W. J. Munro, K. Nemoto, T. C. Ralph, J. P. Dowling, and G. J. Milburn, Rev. Mod. Phys., 2007, 79: 135
9. L. M. K. Vandersypen and I. L. Chuang, Rev. Mod. Phys., 2004, 76: 1037
10. R. Laflamme, E. Knill, D.G. Cory, E.M. Fortunato, T.

Havel, C. Miquel, R. Martinez, C. Negrevergne, G. Ortiz, M.A. Pravia, Y. Sharf, S. Sinha, R. Somma, and L. Viola, arXiv: quant-ph/0207172
11. Y. Makhlin, G. Schön, and A. Shnirman, Rev. Mod. Phys., 2001, 73: 357
12. D. Loss and D. P. DiVincenzo, Phys. Rev. A, 1998, 57: 120
13. J. M. Raimond, M. Brune, and S. Haroche, Rev. Mod. Phys., 2001, 73: 565
14. J. I. Cirac, P. Zoller, H. Kimble, and H. Mabuchi, Phys. Rev. Lett., 1997, 78: 3221
15. A. M. Steane, Phys. Rev. Lett., 1996, 77: 793
16. L. M. Duan and G. C. Guo, Phys. Rev. Lett., 1997, 79: 1953
17. L. Viola, E. Knill, and S. Lloyd, Phys. Rev. Lett., 1999, 82: 2417
18. M. Feng, Phys. Rev. A, 2001, 63: 052308
19. P. G. Kwiat, A. J. Berglund, J. B. Altepeter, and A. G. White, Science, 2000, 290: 498
20. D. Kielpinski, V. Meyer, M. A. Rowe, C. A. Sackett, W. M. Itano, C. Monroe, and D. J. Wineland, Science, 2001, 291: 1013
21. D. M. Greenberger, M. Horne, and A. Zeilinger, Bell's Theorem, Quantum Theory and Conceptions of the Universe, edited by Kafatos M., Dordrecht: Kluwer, 1989: 69
22. W. Dür, G. Widal, and J. I. Cirac, Phys. Rev. A, 2000, 62: 062314
23. H. J. Briegel and R. Raussendorf, Phys. Rev. Lett., 2001, 86: 910
24. R. Raussendorf and H. J. Briegel, Phys. Rev. Lett., 2001, 86: 5188
25. L.-M. Duan, B. Wang and H. J. Kimble, Phys. Rev. A, 2005, 72: 032333
26. L.-M. Duan and H. J. Kimble, Phys. Rev. Lett., 2004, 92: 127902
27. J. Cho and H. W. Lee, Phys. Rev. Lett., 2005, 95: 160501
28. Z. J. Deng, M. Feng and K. L. Gao, Phys. Rev. A, 2007, 75: 024302
29. H. Wei, Z. J. Deng, X. L. Zhang, and M. Feng, Phys. Rev. A, 2007, 76: 054304
30. J. I. Cirac, P. Zoller, H. J. Kimble, and H. Mabuchi, Phys. Rev. Lett., 1997, 78: 3221
31. P. Xue and Y. F. Xiao, Phys. Rev. Lett., 2006, 97: 140501
32. X. F. Zhou, Y. S. Zhang, and G. C. Guo, Phys. Rev. A, 2005, 71: 064302
33. C.H. Bennett, G. Brassard, C. Cr peau, R. Jozsa, A.Peres, and W. K. Wootters, Phys. Rev. Lett., 1993, 70: 1895
34. L. K. Grover, Phys. Rev. Lett., 1997, 79: 325
35. L. K. Grover, Phys. Rev. Lett., 1998, 80: 4329
36. I. L. Chuang, N. Gershenfeld, and M. Kubinec, Phys. Rev. Lett., 1998, 80: 3408
37. J. A. Jones, M. Mosca, and R. H. Hansen, Nature, 1998, 393: 344
38. N. Bhattacharya, H. B. V. van den Heuvell, and R. J. C. Spreeuw, Phys. Rev. Lett., 2002, 88: 137901
39. P. Walther, K. J. Resch, T. Rudolph, E. Schenck, H. Weinfurter, V. Vedral, M. Aspelmeyer, and A. Zeilinger, Nature, 2005, 434: 169
40. H. Wei, R. R. Fang, J. B. Liu, F. Zhou, W. L. Yang, and Z. J. Deng, J. Phys. B, 2008, 41: 085506
41. F. Yamaguchi, P. Milman, M. Brune, J. M. Raimond, and S. Haroche, Phys. Rev. A, 2002, 66: 010302
42. Z. J. Deng, M. Feng, and K. L. Gao, Phys. Rev. A, 2005, 72: 034306
43. M. Feng, Phys. Rev. A, 2001, 63: 052308
44. Z. J. Deng, X. L. Zhang, H. Wei, K. L. Gao, and M. Feng, Phys. Rev. A , 2007, 76: 044305
45. A. Barenco, C. H. Bennett, R. Cleve, D. P. Divincenzo, N. Margolus, P. Shor, T. Sleator, J. Smolin, and H. Weinfurter, Phys. Rev. A, 1995, 52: 3457
46. H. Wei, W. L. Yang, Z. J. Deng, and M. Feng, Phys. Rev. A, 2008, 78: 014304
47. M. Hijlkema, B. Weber, H. P. Specht, S. C. Webster, A. Kuhn, and G. Rempe, Nature Phys., 2007, 3: 253
48. J. A. Sauer, K. M. Fortier, M. S. Chang, C. D. Hamley, and M. S. Chapman, Phys. Rev. A, 2004, 69: 051804
49. A. B. Mundt, A. Kreuter, C. Becher, D. Leibfried, J. Eschner, F. Schmidt-Kaler, and R. Blatt, Phys. Rev. Lett., 2002, 89: 103001
50. J. McKeever, J. R. Buck, A. D. Boozer, A. Kuzmich, H. C. Nagerl, D. M. Stamper- Kurn, and H. J. Kimble, Phys. Rev. Lett., 2003, 90: 133602
51. J. McKeever, A. Boca, A. D. Boozer, J. R. Buck, and H. J. Kimble, Nature, 2003, 425: 268
52. A. Boca, R. Miller, K. M. Birnbaum, A. D. Boozer, J. McKeever, and H. J. Kimble, Phys. Rev. Lett., 2004, 93: 233603
53. Y. L. Lim, A. Beige, and L. C. Kwek, Phys. Rev. Lett., 2005, 95: 030505
54. M. S. Byrd and D. A. Lidar, Phys. Rev. Lett., 2002, 89: 047901
55. L.-A. Wu, M. S. Byrd, and D. A. Lidar, Phys. Rev. Lett., 2002, 89: 127901